Standoff Variation Study II: Detonation of a Donor Munitions Stack and Responses of a Thin Rectangular Water Barricade and an Acceptor Stack

Richard E. Lottero

ARL-TR-1948   May 1999

19990628 044

Army Research Laboratory
Aberdeen Proving Ground, MD 21005-5066

Standoff Variation Study II: Detonation of a Donor Munitions Stack and Responses of a Thin Rectangular Water Barricade and an Acceptor Stack

Richard E. Lottero
Weapons and Materials Research Directorate, ARL

Abstract

This report documents the second stage of the continuation of the fully coupled numerical modeling of the detonation of a simplified munitions stack in a temporary storage area and the subsequent effects on the immediate surroundings of the stack. Three plausible configurations of this munitions stack, referred to as the "donor" stack, an intervening water barricade, and an "acceptor" munitions stack are modeled in two-dimensional (2-D) Cartesian hydrocode computations using the CTH hydrodynamics computer code. The distance between each munitions stack and the barricade, referred to here as the "standoff" distance, is varied from one computation to the next, with the physical characteristics of the munitions stacks and barricade themselves remaining unchanged. The donor stack is modeled as an uncased, condensed high-explosive charge with a rectangular cross section. The water barricade has a relatively thin rectangular cross section, and the acceptor stack is a solid iron rectangle. The loadings on both the barricade and the acceptor stack are computed, as are their fully coupled responses to those loadings. Only a relatively weak inverse functional relationship with standoff distance was found in the barricade response. Weak correlations with both standoff distance and face separation were also found for all parameters that were evaluated for the acceptor stack response, except for the whole-body acceleration. The results are compared with those of the first part of this study on the coupled blast loading and response computations for a massive water barricade with a trapezoidal cross section.

ACKNOWLEDGMENTS

INTENTIONALLY LEFT BLANK

TABLE OF CONTENTS

INTENTIONALLY LEFT BLANK

LIST OF FIGURES

LIST OF TABLES

INTENTIONALLY LEFT BLANK

1. INTRODUCTION

This report documents the continuation of a study of the detonation of a single munitions stack within a postulated munitions temporary storage area and the subsequent effects on its surroundings. The terminology for the main features that are modeled in the storage area are the same as before.[1, 2] The detonating munitions stack is referred to as the "donor" stack; the remaining munitions stacks that are in the storage area and subject to blast loading from the donor stack are the "acceptor" stacks; a postulated, field-expedient, protective wall between any two munitions stacks is the "barricade;" and the distance from the base of a munitions stack to the base of a barricade is the "standoff" distance. As stated before, the primary purpose of protective barricades is to prevent a direct, line-of-sight path from existing for either blast or fragments between munitions stacks in proximity to one another. Additionally, the impact of any part of a barricade on an acceptor stack must not be capable of initiating an exothermic reaction in the acceptor stack. This computational study is one part of a larger study by the U.S. Army Research Laboratory (ARL) on behalf of its customer, the U.S. Army Defense Ammunition Logistics (Ammolog) Activity. This part involves a computational analysis of the dynamics of a detonating munitions stack and the effectiveness of field-expedient barricades in preventing a subsequent chain reaction among acceptor stacks.

The logic for considering the development of field-expedient barricades was given as follows.[2]

> Military units operating in rapidly changing situations typically cannot store munitions using standard safe-distance guidelines normally applicable for permanent storage in a safe area. Munitions must be readily accessible either for use or relocation with minimal delay. At times such as these, it is sometimes considered necessary by commanders in the field to store munitions in closely spaced stacks in the open with no protective barricades between them. An incidence of extremely close spacing of munitions stacks with no barricading that occurred in the buildup of ammunition stocks at the port of Al Jubayl, Saudia Arabia, before the opening of hostilities in the Gulf War was cited in an earlier report[1] [same reference number in both reports]. Fortunately, no initiating incident occurred. The same earlier report included, as examples of what can occur, photographs showing some of the destruction at Doha, Kuwait, in 1991 after a fire started a chain reaction among unprotected, closely spaced munitions stacks.

The first study of the effects of standoff variation on the loading and response of the acceptor stack was done for a massive water barricade having a trapezoidal cross section.[2] It showed that the sloping sides of the trapezoidal water barricade were effective in deflecting blast and explosive products upward and away from the acceptor stack. The normalized blast loading on the trapezoidal barricade and its whole-body response were relatively weak functions of the inverse of the normalized standoff distance. An analysis of the blast and

impact loading on the acceptor stack showed that it was a three-stage process, with the first stage from the air blast, and the next two stages from a water wave at the top of the barricade and then the impact of the lower section of the barricade. The blast loading on the acceptor stack was negligible, and the normalized impact loading of the water barricade on the acceptor stack had a nearly one-to-one correspondence with the inverse of the normalized standoff distance. The five standoff distances in this first fully coupled computational[2] study were 3.048 m (10.0 ft), 2.75 m (9.02 ft), 2.50 m (8.20 ft), 2.25 m (7.38 ft), and 2.00 m (6.56 ft).

This report describes a series of fully coupled computations for three different standoff distances: Computation 980825 for a 3.048-m (10.0-ft) standoff (hereinafter rounded to 3.05 m for simplicity except when specifically used to calculate a parameter), Computation 980826 for a 2.50-m (8.20-ft) standoff, and Computation 980827 for a 2.00-m (6.56-ft) standoff. The donor stack and acceptor stack are modeled in a way that is identical to that used in the previous studies.[1, 2] The barricade is modeled as a simple rectangle having the same height as both the donor and acceptor stacks and, therefore, the same height as the trapezoidal barricade in the previous studies. All computations are fully coupled in the sense that the detonation of the munitions stack; the blast loading on and response of the barricade; and loading from all sources on and the response of acceptor stack are modeled in a single, continuous computation.

2. COMPUTATIONAL APPROACH AND GEOMETRY

2.1. The Hydrocode Model

The three coupled computations that are reported here were performed using the then-latest general-release version, CTH_9801, of the CTH[3] hydrocode developed at Sandia National Laboratories (SNL). It also includes the May 1998 and August 1998 "patches" (i.e., coding updates) that were released by SNL. CTH solves the inviscid Euler equations using a second-order accurate, explicit time-stepping method. A brief description of the CTH hydrocode was given in the previous report.[2] The reader is referred to McGlaun et al.[3] for a full discussion of the CTH hydrocode, and to the appropriate users' manuals for practical information about the structure and use of the CTHGEN[4] grid generation code, the CTH[5] hydrocode, and their supporting utilities.

The three computations presented here were performed using the two-dimensional (2-D) Cartesian coordinates system option in CTH, just as was done for the previous computations. The choice of 2-D Cartesian coordinates meant that the computations provided a worst-case blast loading for the simplified, uncased charge of condensed high explosives by eliminating the possibility of having any compression or expansion waves in the direction of depth of the munitions stacks and barricade. (Depth is a measure parallel to both the ground and the side walls of the munitions stack, and normal to the page in the flow field plots shown later.) In effect, the donor and acceptor stacks and the barricade have an infinite depth

in that coordinate system. In the CTH hydrocode model, which uses the centimeter-gram-second (cgs) units system, this implies a unit depth of 1.0 cm. The same gridding was used. The nominal computational cell dimensions are 4.0 cm in both Δx (width) and Δy (height). These computations were performed on the Silicon Graphics, Inc., (SGI) Origin 2000 unclassified computers at the ARL Major Shared Resource Center (MSRC) at Aberdeen Proving Ground (APG), MD. This is one of four MSRCs in the United States that are administered by the High Performance Computing Modernization Office (HPCMO). Each of these 2-D Cartesian computations took about 250,000 central-processor-unit (cpu) seconds.

2.2. The Donor Munitions Stack

The donor stack is modeled the same as in the previous reports,[1, 2] as an uncased charge with no packing materials. This reduced the analysis to one of blast loading only, with no production of fragments or other debris. The explosive mass of the donor stack is modeled as a single, condensed charge rather than as a distributed set of smaller condensed charges. The choice of the munitions in the donor munitions stack was made by consulting a previous ARL report on fragment propagation probabilities by Starkenberg et al.[6] The donor munitions stack was assumed to be of the same size as one consisting of 72 pallets of M107 155-mm projectiles, stacked three pallets high by four wide by six deep. Each pallet contains eight rounds. The dimensions of this particular stack are 2.44 m high by 2.94 m wide by 2.19 m deep (8.00 ft by 9.63 ft by 7.20 ft). A single M107 round can contain either 6.62 kg (14.6 lbm, where "lbm" denotes pounds mass, avoirdupois) of TNT or 6.98 kg (15.4 lbm) of Composition-B (hereinafter referred to as "Comp-B"). The total mass of a pallet, including packaging, is 362 kg (797 lbm).[7] Thus, a presumed stack of M107 munitions would contain 576 rounds, having a total mass of Comp-B equal to 4,024 kg (8,870 lbm). For simplicity, the nominal explosive mass of Comp-B for this computational study was taken as 4,000 kg (8,818 lbm) for the donor stack, the regulatory maximum.[8] The total mass of an actual stack containing 72 pallets of M107 rounds is 26,029 kg (57,384 lbm), including all packaging materials. This equates to a mass of 118.61 kg/cm of depth for the actual stack with all materials considered. The acceptor stack was assumed to be of the same physical dimensions and total mass as those of the donor stack.

The explosive modeled was Comp-B, taken at its reference density of 1.72 g/cm^3 in its undetonated state, and modeled[9] within the Sesame[10] equation-of-state (EOS) package. The SNL Sesame EOS package includes tabular data for high explosives and separate implementations of data for the Mie-Gruneisen, Jones-Wilkins-Lee (JWL), and ideal-gas equations of state. The explosive charge was placed within the computational flow field with its center coincident with that of the M107 donor stack described before. After assigning the donor stack the nominal explosive mass of 4,000 kg and using the actual stack depth of 2.19 m, this equated to an explosive charge mass of approximately 18.227 kg/cm of depth of the stack to be modeled in the unit-depth 2-D Cartesian coordinates flow field in CTH. This mass of Comp-B was modeled as a rectangle whose width and height were in direct proportion to

those for the donor stack. Specifically, the explosive charge was 93.91 cm high and 113.04 cm wide (i.e., the full width, and not one-half width for symmetry), located with its center of mass 121.92 cm above the ground plane. The ground plane was designated as a frictionless, perfectly reflective boundary.

A small central section of the explosive charge at the left symmetry boundary served as a computational "booster" charge. It was detonated using the programmed burn[4] model using a constant detonation velocity 7.98 km/s for reference-density Comp-B.[11] This model simulates the complete detonation of any part of an explosive charge that is passed by the expanding theoretical detonation front moving at that constant velocity. The remainder of the detonation was modeled using the "history variable reaction burn" (HVRB) model.[10] The HVRB model evaluates the thermodynamic state of a mass of undetonated explosive in a given computational flow field cell to determine if that material should be detonated in that time step. The detonation initiation point was located at the center of the explosive charge at the (X,Y) point (0.0, 121.92 cm).

2.3. The Barricade

The barricade shape chosen for the computations is a simple rectangle with a nominal height of 2.44 m (8.0 ft), the same height as that for the munitions stacks and for the trapezoidal barricade studied previously.[2] The width chosen for this thin rectangular barricade is equal to the average width (measured front face to back face in the 2-D terminology used in this report) of a sand-filled Concertainer barricade, marketed by Hesco Bastion Limited[12] that was tested against a detonated pallet of M107 rounds for ARL[13] by the Aberdeen Test Center (ATC). The actual measurements of the sand-filled Concertainer barricade were taken at several points,[14] giving an average width of 1.173 m (46.2 in) (hereinafter rounded to 1.17 m for brevity). Other than using this nominal value for the width of the rectangular water barricade, the rectangular water barricade simulated in the computations reported here has no relation, direct or indirect, to Concertainer or any other product by Hesco Bastion. Any data related to or evaluation of the rectangular water barricade simulated here also should not be construed as having any relation to any commercial product by Hesco Bastion. An idealized cross section that has no internal air spaces and consists only of water is assumed. No construction or supporting materials are considered. The mass of water for the barricade is 28.61 kg/cm of depth. The water in the barricade was modeled using the CTH Sesame EOS for water.[15] The face of the barricade closest to the donor stack was placed at the defined standoff distance, which varied from 3.05 m (10 ft) to 2.00 m (6.56 ft), from the nearest side of the donor stack. The standoff distance here is measured from the face of what would have been the actual side of the donor munitions stack, not the condensed explosive charge representing the stack.

4

2.4. The Acceptor Munitions Stack

The acceptor munitions stack was modeled in all computations as a simple, relatively inert mass of iron[16] with the same height (2.44 m) and width (2.94 m) as the reference M107 munitions stack. This is identical to the way the acceptor stack was modeled in all previous[1, 2] computations. The acceptor stack in each computation was located at a standoff distance equal to that between the donor stack and the barricade. The purpose in modeling the acceptor stack as a full-sized mass of iron was for the convenience of having a massive, relatively non-responding object with the correct physical dimensions in order to observe wave interactions on the surface and to provide surface blast loading data through the use of CTH's "tracer" particles placed in the air near the surfaces. Tracer particles are massless points that are specified at desired locations by the user at grid generation time. They may be fixed in computational space or be free to move along one or more of the principal axes in the grid. A relatively full complement of data describing the thermodynamic state and other physical parameters at the location of each tracer is recorded for later processing by the user. When analyzing the whole-body response of the acceptor stack later in this report, the correct acceptor stack mass (118.61 kg/cm of depth) was used to compute the motion of the acceptor stack from the X-direction momentum of the massive iron stack. Some of the details of the blast development in this computational series and subsequent interactions between the blast and the barricade and then the barricade and the acceptor stack are surely artifices of the simplified geometries, but the overall dynamics appear to be quite reasonable.

3. THE HYDROCODE COMPUTATIONS

3.1. Flow Field Development

Computation 980825 simulated a fully coupled blast and impact loading sequence at a standoff of 3.05 m (10.0 ft). Even though the standoff is the same as that in Computation 980505,[2] there are two very significant differences in the barricades beyond the obvious difference in the cross sections and slopes of the left and right faces. The trapezoidal water barricade mass is 58.71 kg/cm of depth with an X-direction distance of its center of mass equal to 4.96 m from the right face of the donor stack. The rectangular water barricade has a mass of 28.61 kg/cm of depth with an X-direction distance of its center of mass equal to 3.63 m from the right face of the donor stack. Thus, the rectangular water barricade has approximately 0.49 times the mass of the trapezoidal barricade, and has the distance of its center of mass from the donor stack right face at 0.73 times that for the trapezoidal barricade. Figure 1 shows the computational flow field at the start of Computation 980825 at the instant of the initiation of the detonation (hereinafter referred to as "initiation") with time defined to be equal to zero. The "Y" axis at the left of the figure represents the height measured from the ground plane. In this simple 2-D Cartesian coordinate system, the left boundary at the Y axis is designated as a frictionless, perfectly reflective plane of

symmetry. The "X" axis represents the measure of width in the system and coincides with the frictionless, perfectly reflective ground plane. The Y axis at the X = 0.0 location is also a vertical bisector of the donor stack. The air in the flow field, modeled with data from Graboske[17] within the Sesame[10] EOS package, is shown with the color yellow. The top and right transmissive boundaries are marked by the top and right edges of that yellow region. These transmissive boundaries were designated as zero-gradient, outflow-only boundaries to minimize the possibilities of generating spurious, mathematically generated reflected waves or inflows when those boundaries are struck by large-gradient outflows. The explosive charge representing the donor stack is shown as the red (one-half) rectangle on the left symmetry boundary, the water barricade is shown as the blue rectangle, and the acceptor stack is shown as the black rectangle (the object closest to the right transmissive boundary). These settings and general descriptions, except for the shape of the barricade, are the same as for the previous series[2] of computations. In order to facilitate direct comparison of the flow fields for the 3.05-m standoff for the rectangular versus the trapezoidal barricade, flow fields from Computation 980505[2] are also presented. Figure 2 shows the flow field at the instant of initiation for Computation 980505 for the trapezoidal barricade. A comparison between Figures 1 and 2 clearly shows the greater actual spacing and mass of the trapezoidal barricade.

Figure 3 shows the computational flow field for 980825 at 5.0 ms after the initiation of the donor stack. The detonation process had already been completed by this time (theoretically at 0.092 ms). The expanding explosive products and leading shock have deformed and accelerated the barricade. A section of the expanding explosive products has already passed over the acceptor stack. The lower section of the barricade is translating laterally toward the acceptor stack as a relatively unified block. Much of the top section of the water barricade has deformed into an S-shaped curve, with all but the top-most part of it trailing behind the lower section. As yet, no part of the barricade appears to have arrived at the left face of the acceptor stack, and no explosive products appear to have reached the acceptor stack. For comparison, Figure 4 shows the computational flow field for 980505 at 5.0 ms after the initiation of the donor stack. The more massive trapezoidal water barricade in that computation is also showing the leading action of the lower section of the barricade, but with a different set of dynamics. The leading section is a manifestation of a growing wave that travels up the right face of the barricade, as described previously.[2] It is also considerably farther from the accepter stack left face at this time than the lower, leading section of the rectangular barricade shown in Figure 3.

Figure 5 shows the computational flow field at 7.5 ms after the initiation of the donor stack. The barricade is already in the process of impacting the left face of the acceptor stack along its entire height. Figure 6, on the other hand, shows the flow field for the trapezoidal barricade computation at the same time. The bottom-to-top wave on the right face of the barricade is still in the early stage of its development, with its rightward leading edge still more than 2 m away from the acceptor stack left face.
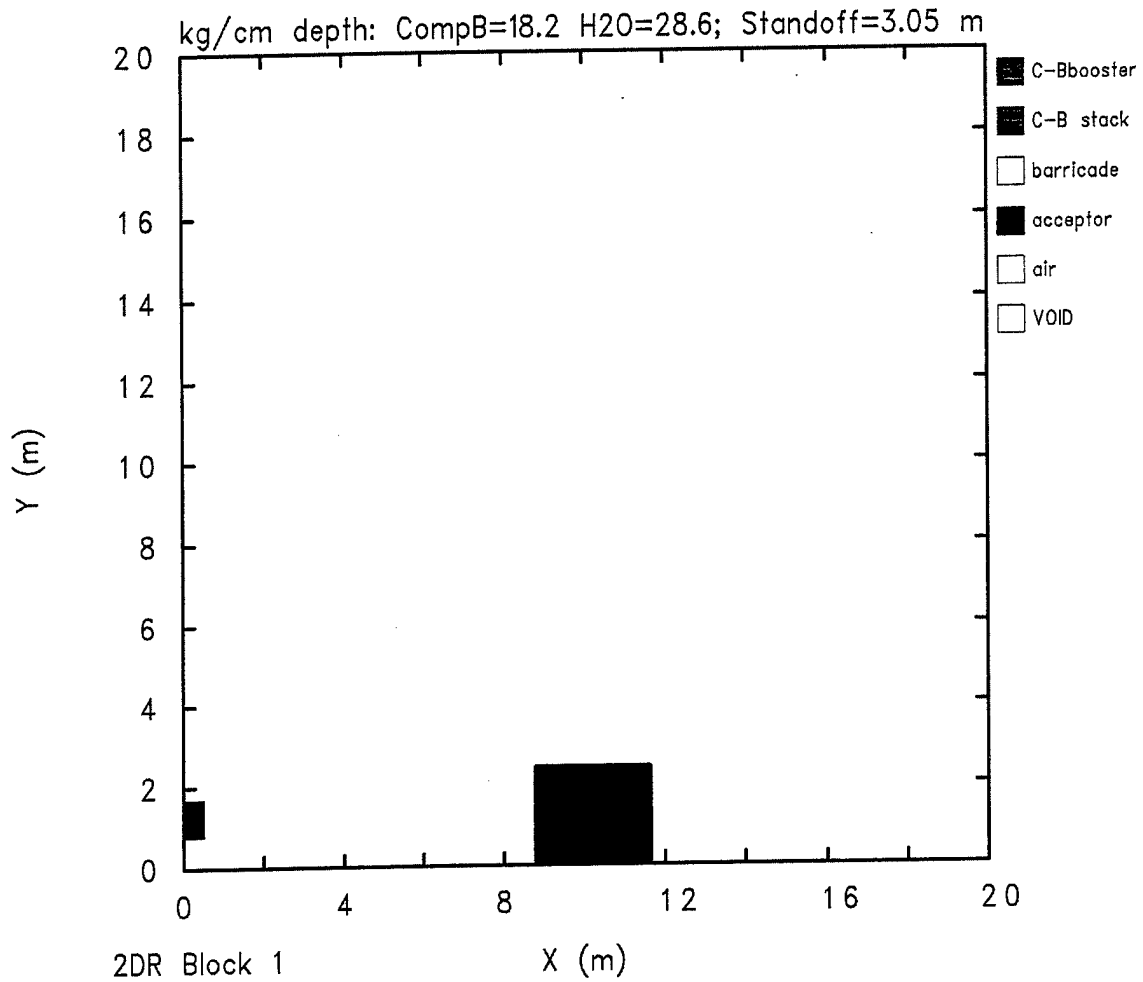
Figure 1. Flow Field at Time = 0.0 for Computation 980825, 3.05-m Standoff, Thin Rectangular Barricade.
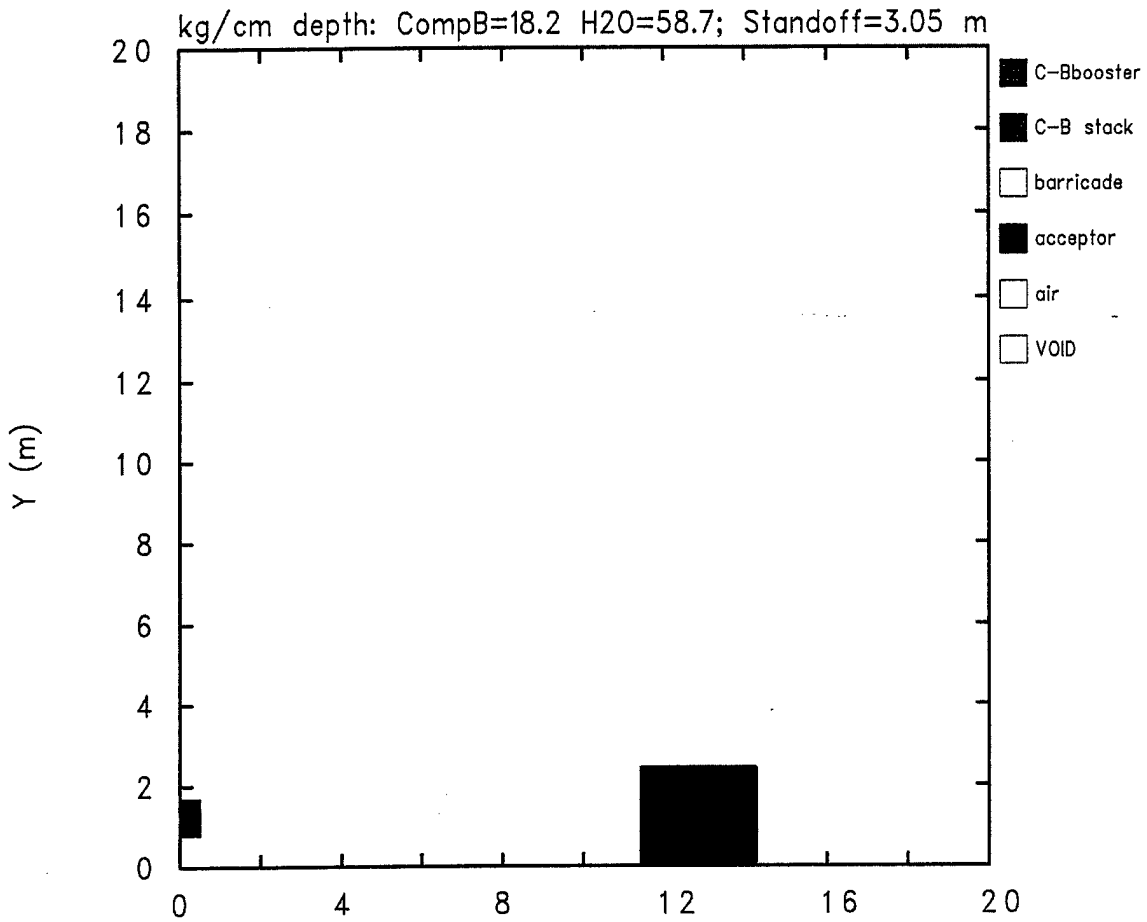
Figure 2. Flow Field at Time = 0.0 for Computation 980505, 3.05-m Standoff, Massive Trapezoidal Barricade.
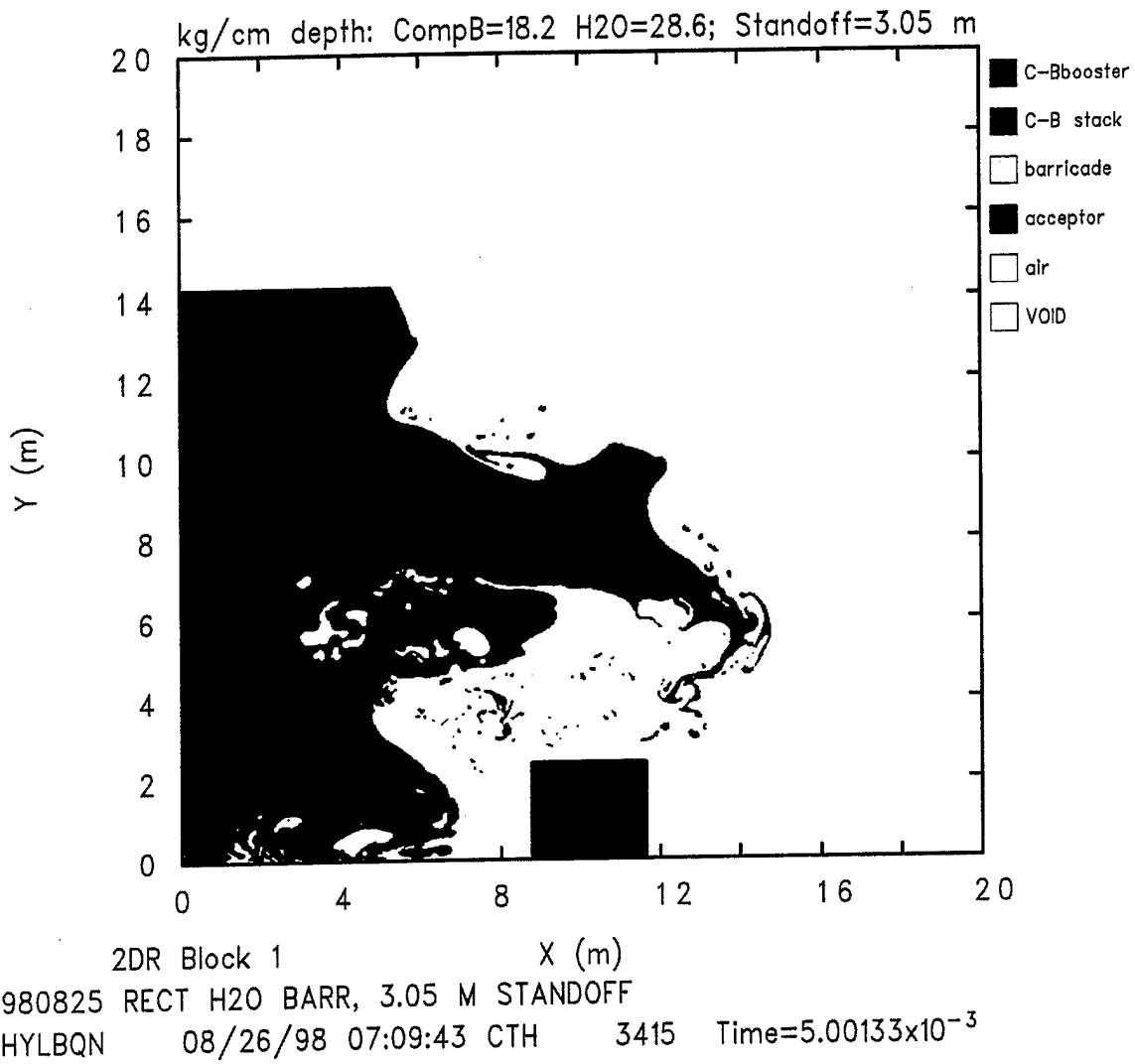
Figure 3. Flow Field at Time = 5.0 ms for Computation 980825, 3.05-m Standoff, Thin Rectangular Barricade.
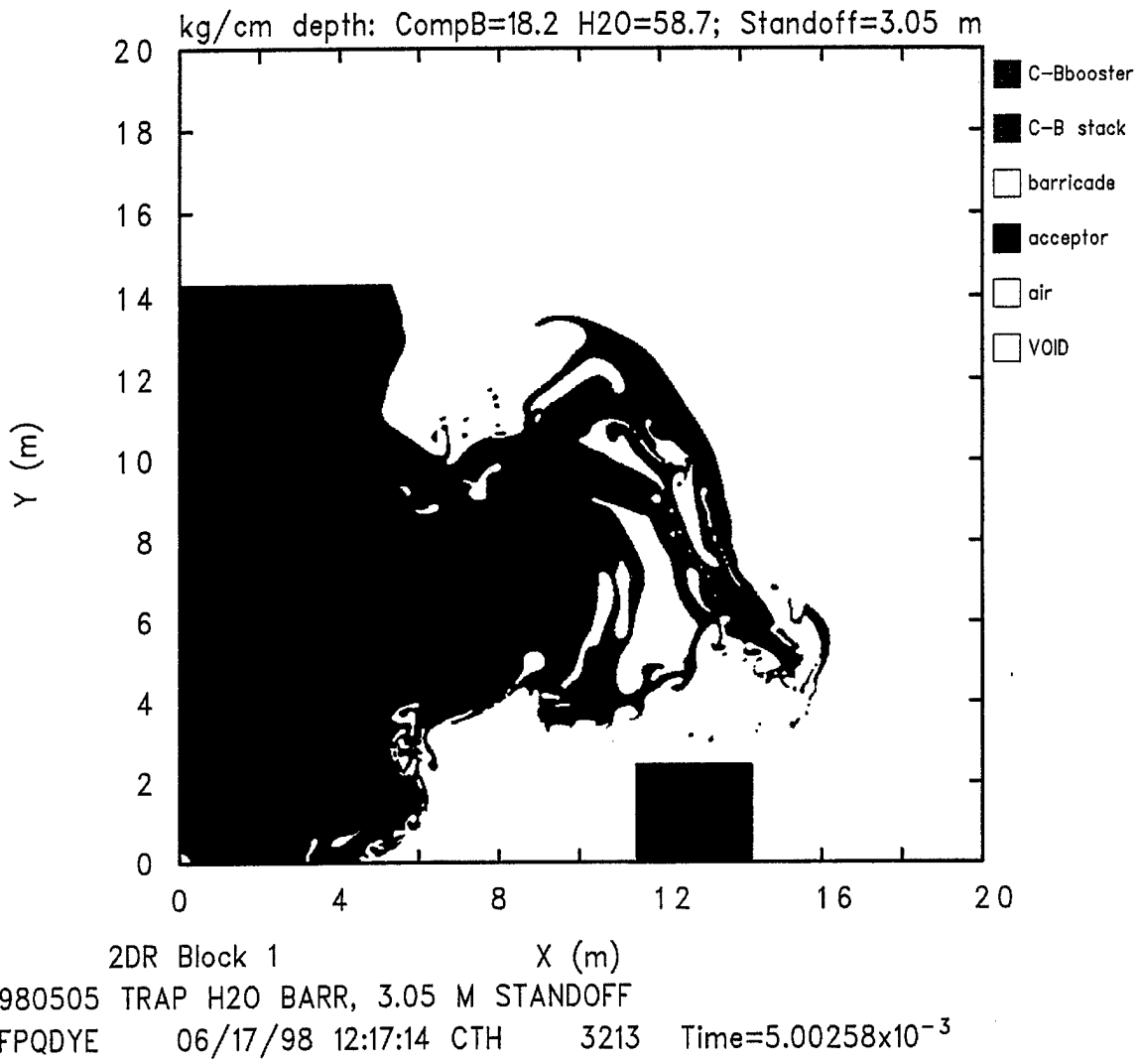
Figure 4. Flow Field at Time = 5.0 ms for Computation 980505, 3.05-m Standoff, Massive Trapezoidal Barricade.

Figure 5. Flow Field at Time = 7.5 ms for Computation 980825, 3.05-m Standoff, Thin Rectangular Barricade.

Figure 6. Flow Field at Time = 7.5 ms for Computation 980505, 3.05-m Standoff, Massive Trapezoidal Barricade.

Figure 7 shows the computational flow field at 10.0 ms after initiation. The portion of the barricade that impacted the left face of the acceptor stack has rebounded from it and is moving in the negative X direction. The remainder of the barricade has been dispersed upward and away from the acceptor stack. Some explosive products are relatively close to the top-rear corner of the acceptor stack, and some are approaching the bottom-left corner. Figure 8 for 980505 shows continued development of the wave on the right surface of the barricade, with its rightward-leading tip still more than 1 m away from the acceptor stack.

Figure 9 shows that, by 12.5 ms after initiation, the thin rectangular barricade no longer has any useful structural integrity and no readily recognized shape. A small amount of explosive products appears to be making contact with the lower-left corner of the acceptor stack, and a large region of explosive products seems to be moving very close to the top-left corner of the stack. In contrast, Figure 10 shows that for the trapezoidal barricade, the leading wave of water is still about 0.7 m away from impacting the acceptor stack and the barricade is still maintaining a distorted but relatively integral shape. No explosive products are in the immediate vicinity of the acceptor stack.

Figure 11 shows the computational flow field for the rectangular barricade at 15.0 ms after initiation. The barricade has been reduced to simply being widely distributed water, with some of it already swept out of the computational grid. Explosive products are close to portions of the left and top faces of the acceptor stack. Figure 12, which shows the flow field for the trapezoidal barricade in Computation 980505, shows a distorted but still-intact barricade with the tip of the wave on its right-rear face almost at the point of its first contact with the left face of the acceptor stack. Most of the air blast and virtually all of the explosive products have been deflected upward and away from the acceptor stack by the trapezoidal barricade.

Figure 13 shows the computational flow field at 20.0 ms after initiation. Much of the top face of the barricade has contact or near-contact with explosive products, as does its lower-left corner. Some explosive products are nearing the back face. Figure 14 for 980505 shows the first interaction of water from the wave on the right face of the trapezoidal barricade with the top section of the acceptor stack. The barricade is still largely intact, and no explosive products are near the surfaces of the acceptor stack.

Progressing further in time, Figure 15 shows the computational flow field for the thin rectangular barricade at 30.0 ms after initiation. The removal of the remaining water from the barricade from the computational flow field is nearly complete. Much of the left face of the acceptor stack, most of the top face, and small parts of the right face appear to be in contact with explosive products. Figure 16 shows the flow field for 980505. The interaction of the barricade with the left surface of the acceptor stack is continuing, with the peak overpressure loadings on the acceptor stack yet to occur. The air gap at the bottom of the left face of the acceptor stack is still being compressed by the oncoming water from the barricade. The now-distributed but still-intact barricade is serving as a protective barrier by continuing to keep explosive products away from the acceptor stack faces.

13

kg/cm depth: CompB=18.2 H2O=28.6; Standoff=3.05 m

Legend:
- C-Bbooster
- C-B stack
- barricade
- acceptor
- air
- VOID
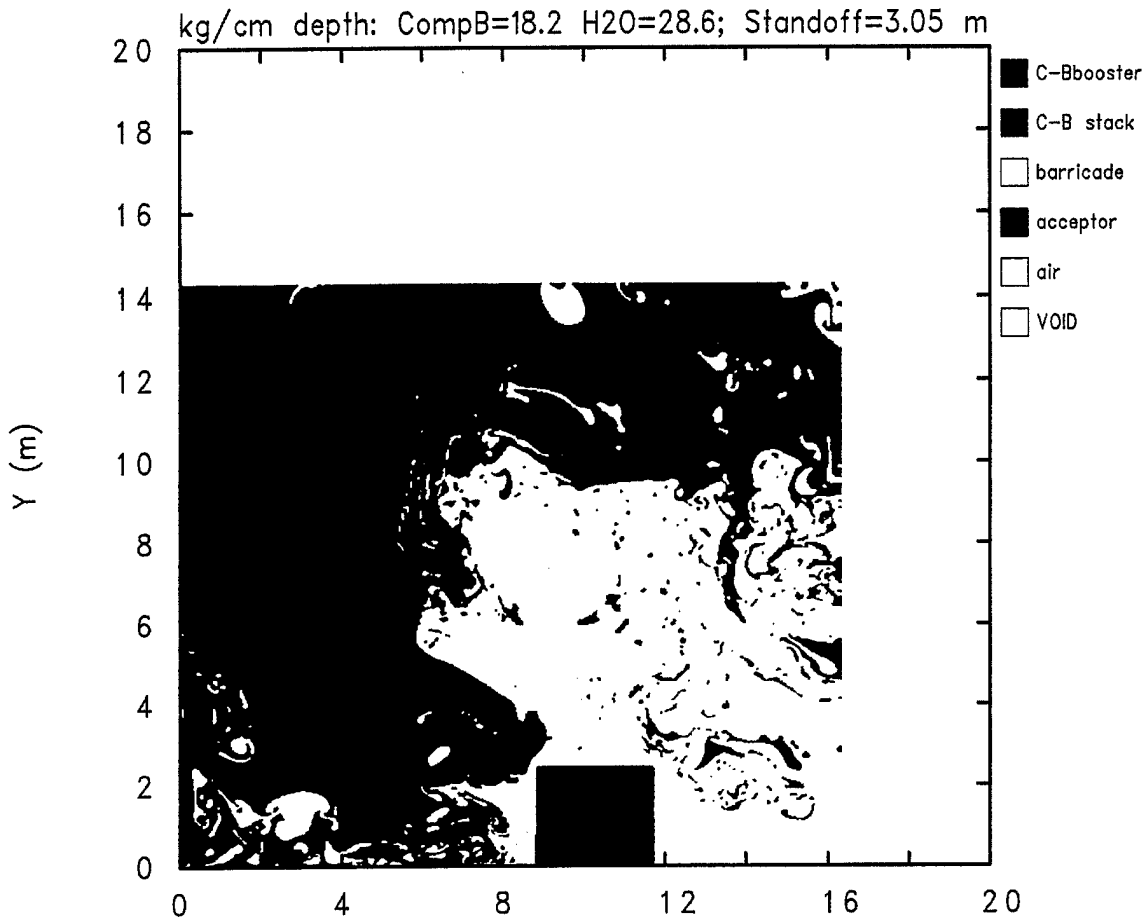
2DR Block 1 X (m)
980825 RECT H2O BARR, 3.05 M STANDOFF
HZQCNJ   08/26/98 20:36:48 CTH   5746   Time=1.00003x10^{-2}

Figure 7. Flow Field at Time = 10.0 ms for Computation 980825, 3.05-m Standoff, Thin Rectangular Barricade.

kg/cm depth: CompB=18.2 H2O=58.7; Standoff=3.05 m
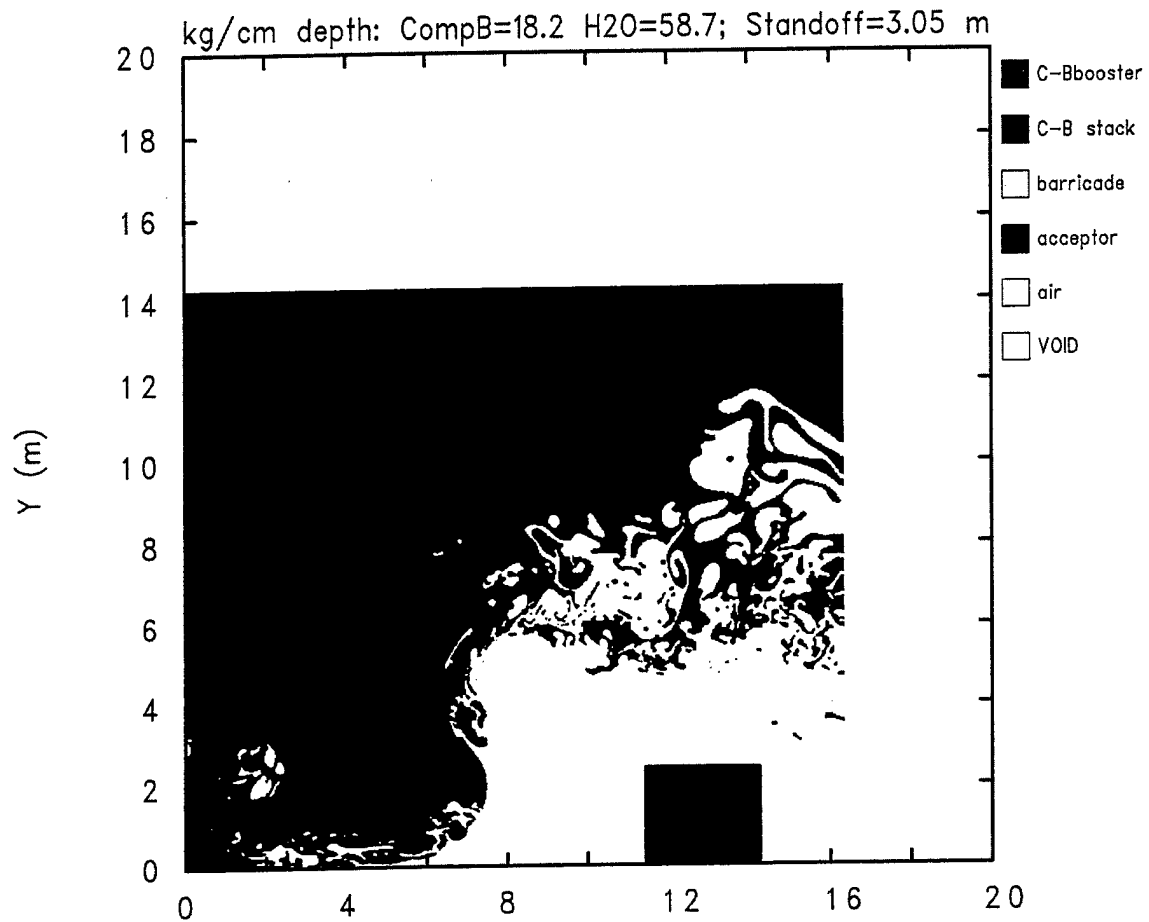
Figure 8. Flow Field at Time = 10.0 ms for Computation 980505, 3.05-m Standoff, Massive Trapezoidal Barricade.

Figure 9. Flow Field at Time = 12.5 ms for Computation 980825, 3.05-m Standoff, Thin Rectangular Barricade.
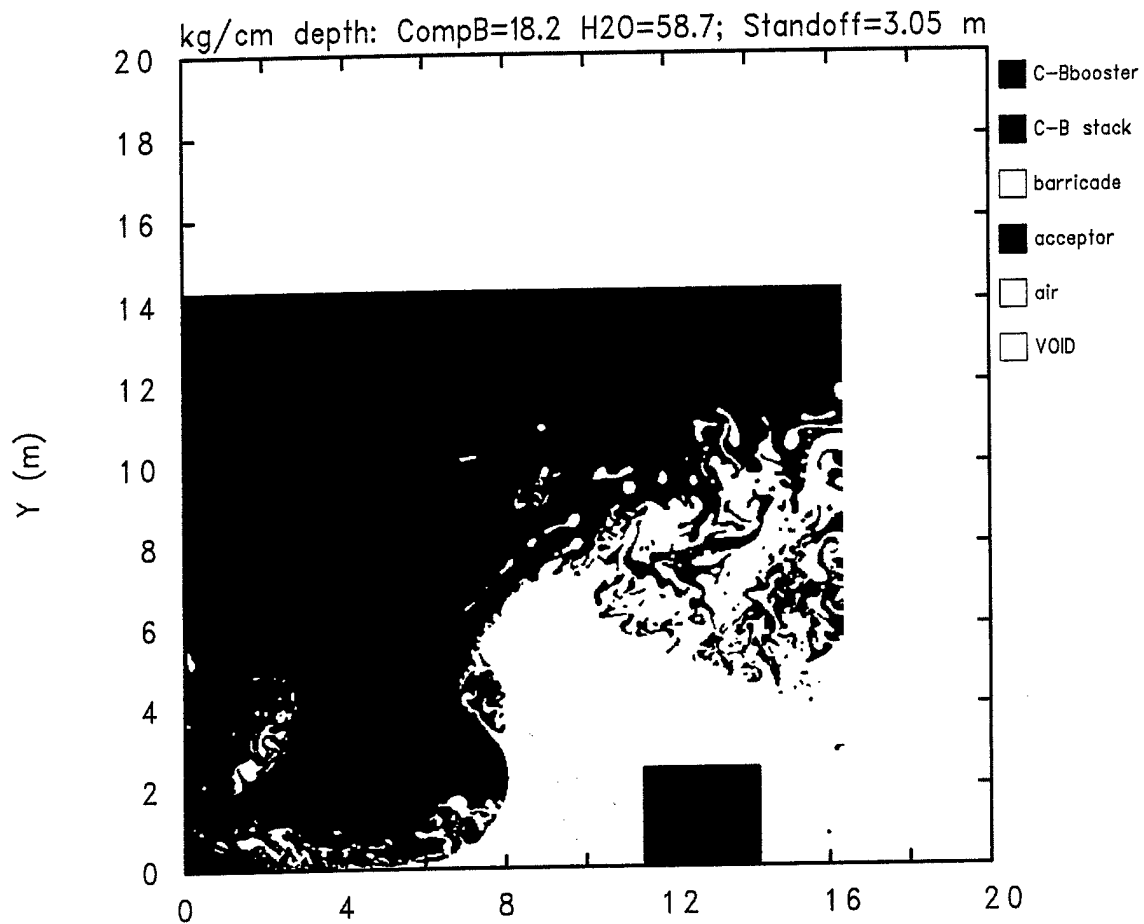
Figure 10. Flow Field at Time = 12.5 ms for Computation 980505, 3.05-m Standoff, Massive Trapezoidal Barricade.
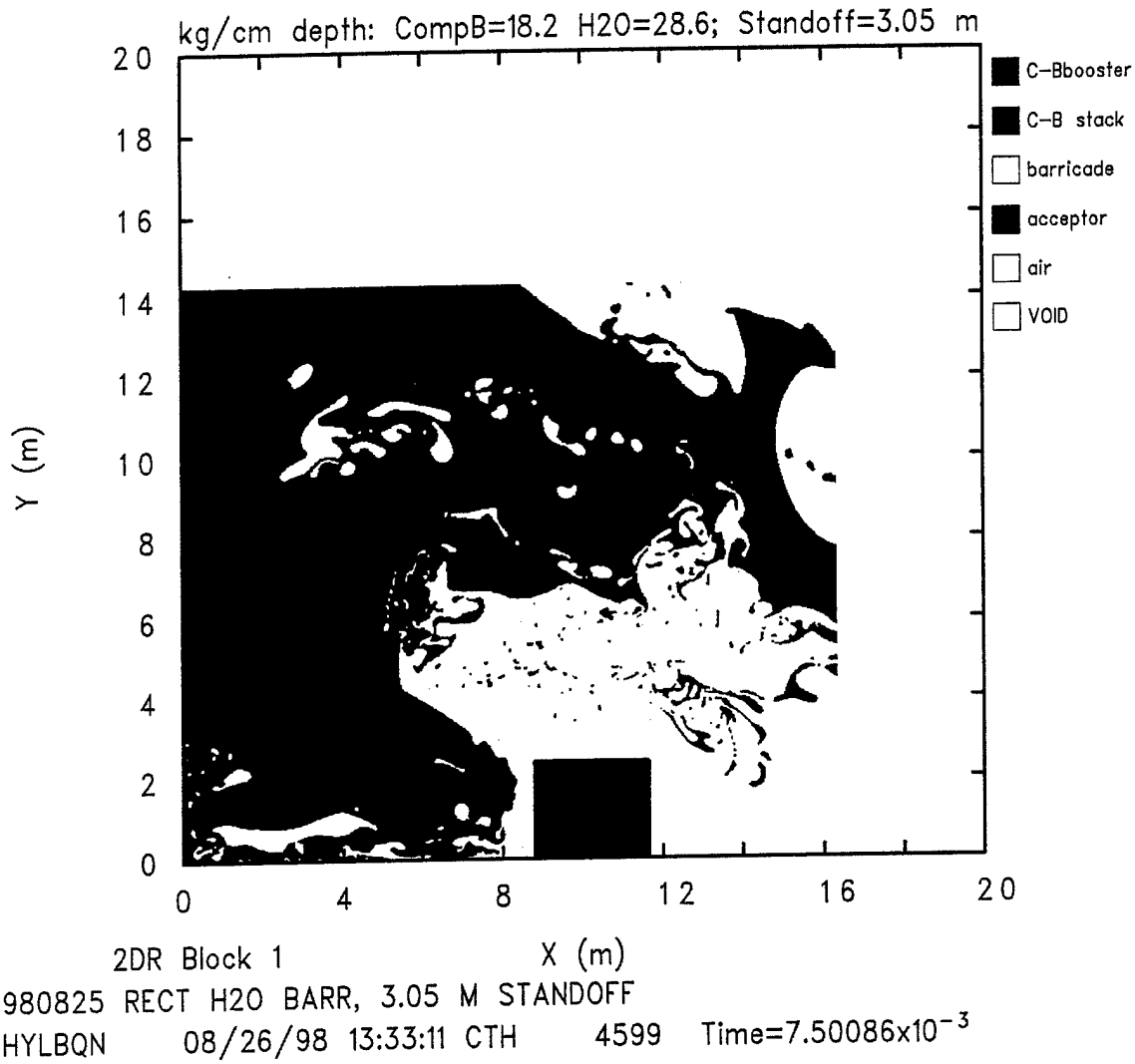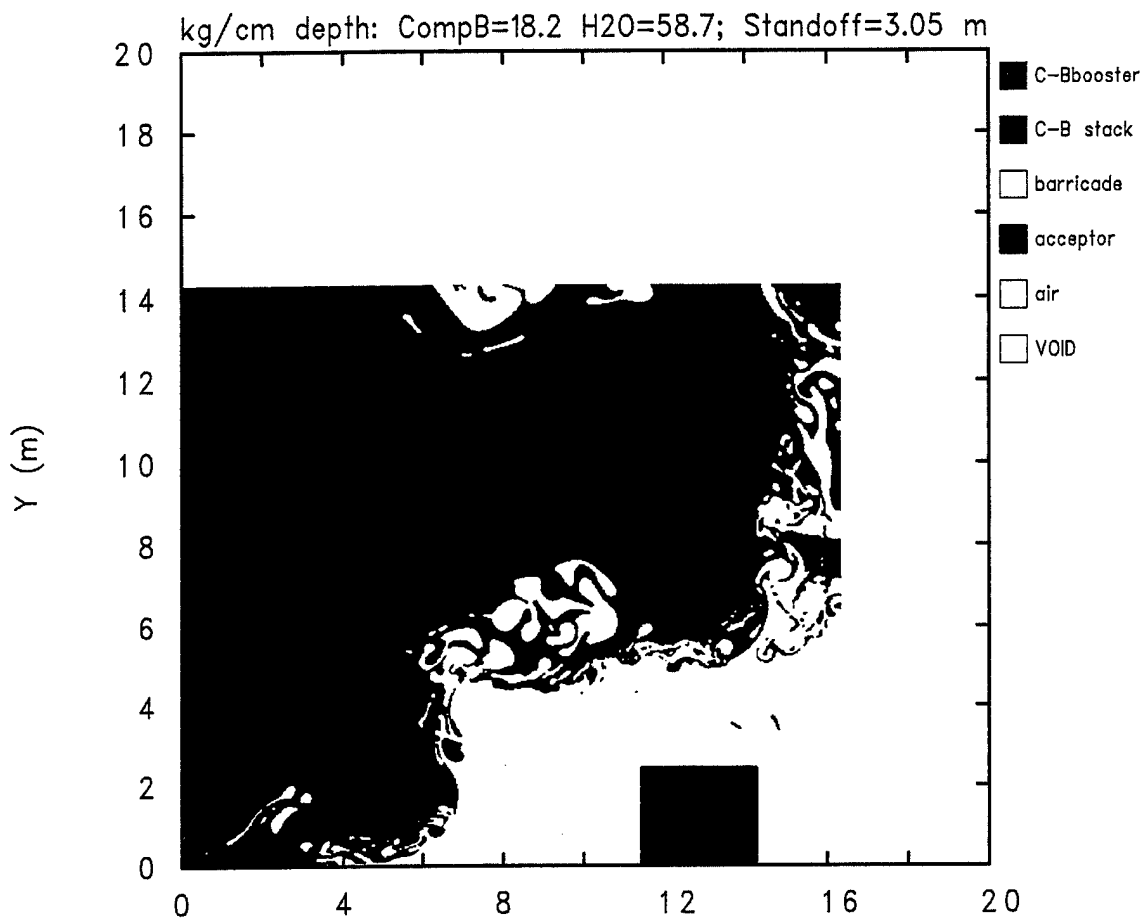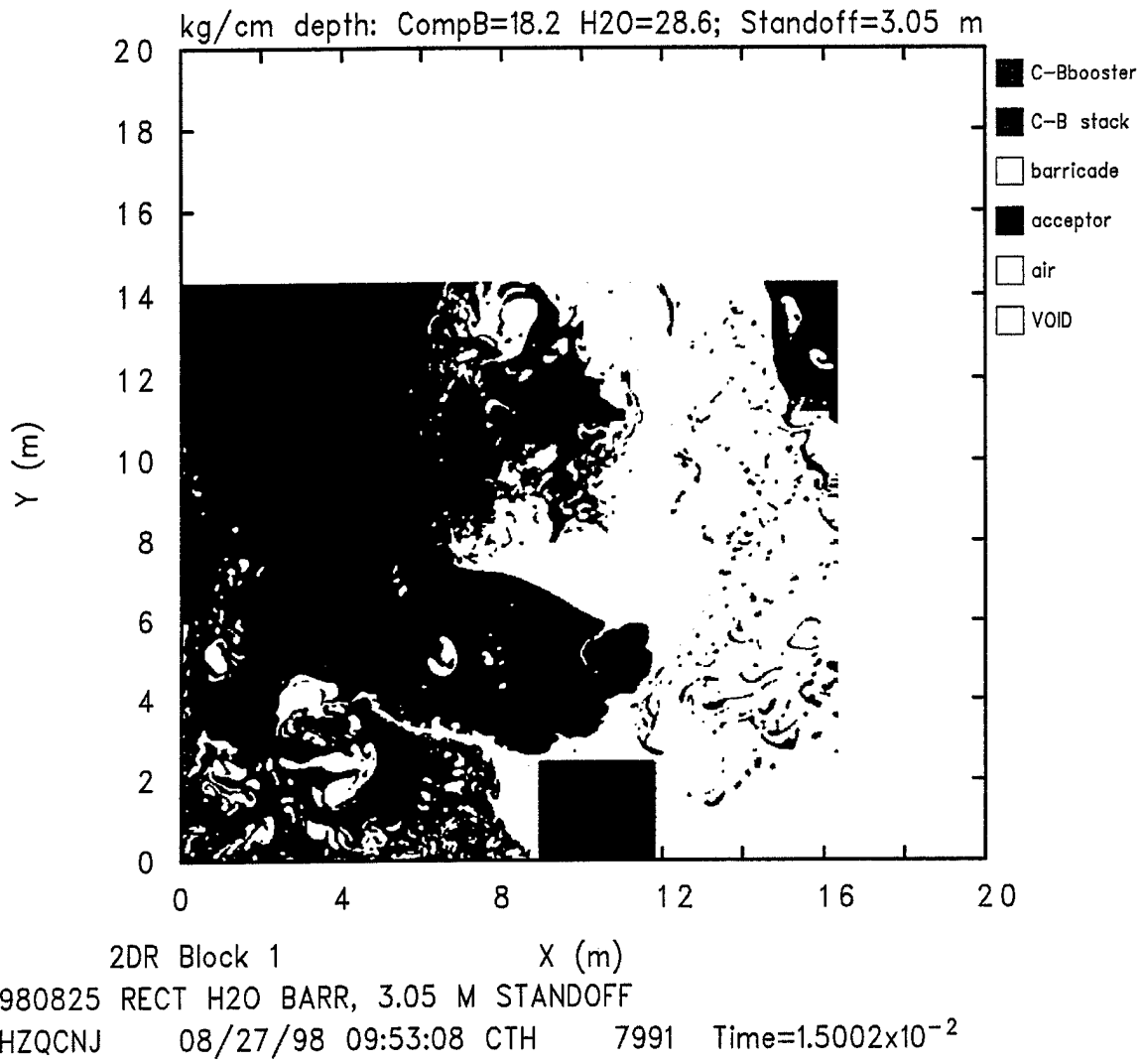
Figure 11. Flow Field at Time = 15.0 ms for Computation 980825, 3.05-m Standoff, Thin
Rectangular Barricade.
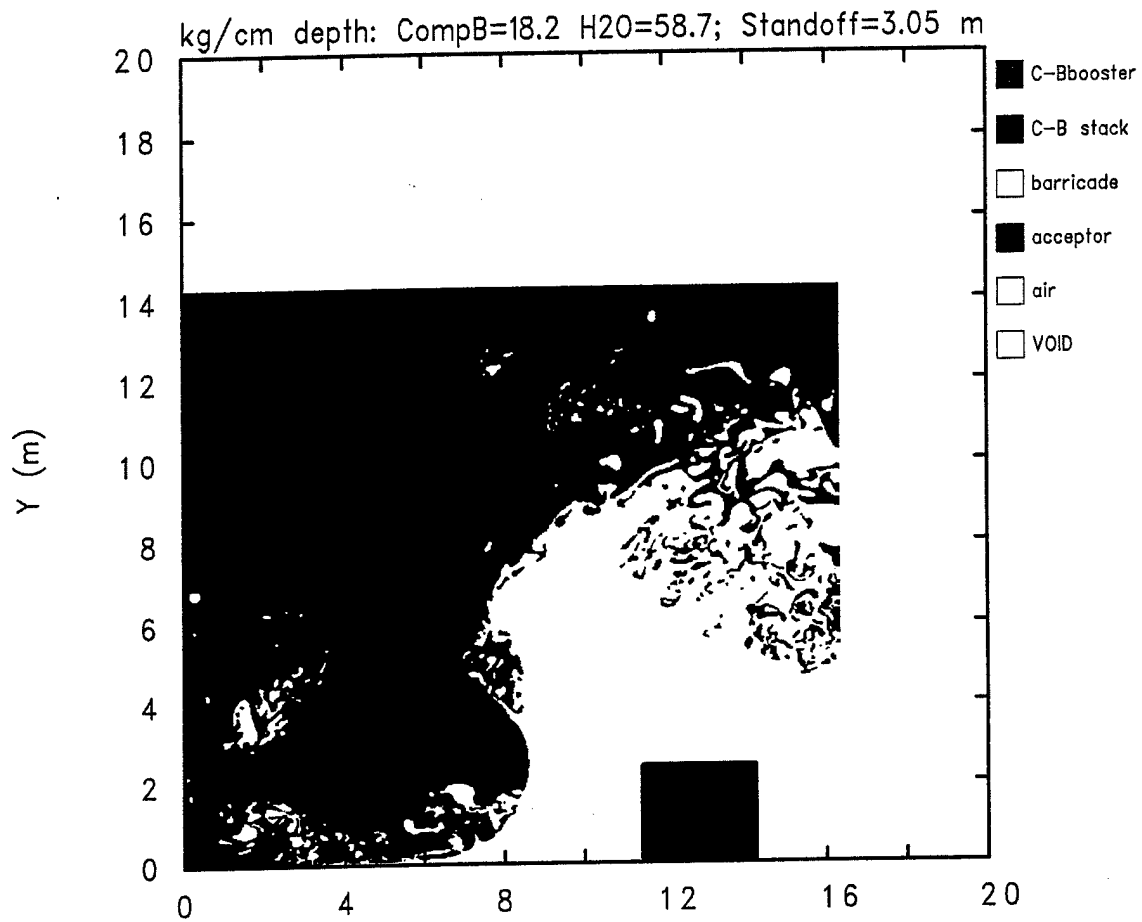
Figure 12. Flow Field at Time = 15.0 ms for Computation 980505, 3.05-m Standoff, Massive Trapezoidal Barricade.

Figure 13. Flow Field at Time = 20.0 ms for Computation 980825, 3.05-m Standoff, Thin Rectangular Barricade.
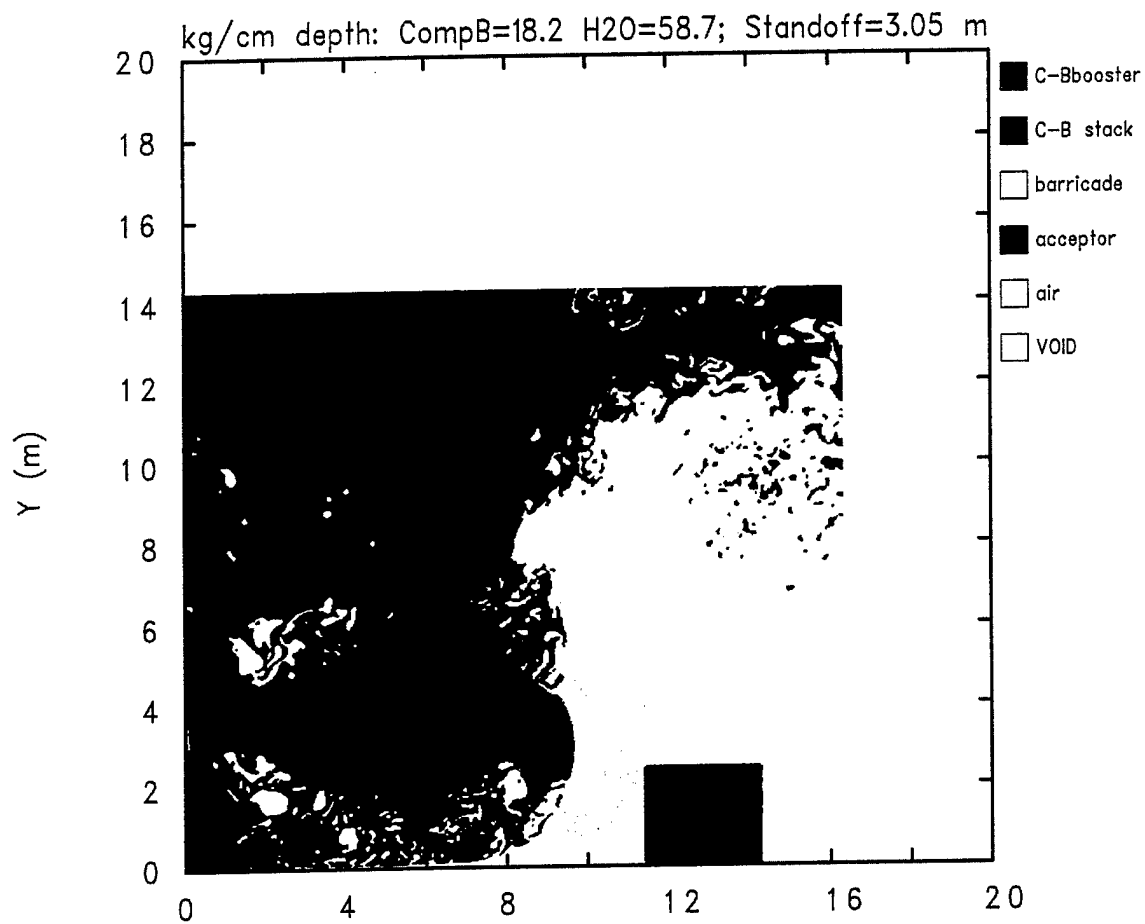
Figure 14. Flow Field at Time = 20.0 ms for Computation 980505, 3.05-m Standoff, Massive Trapezoidal Barricade.

kg/cm depth: CompB=18.2 H2O=28.6; Standoff=3.05 m

Legend:
- C-Bbooster
- C-B stack
- barricade
- acceptor
- air
- VOID

2DR Block 1   X (m)
980825 RECT H2O BARR, 3.05 M STANDOFF
HOPAIV   08/28/98 16:27:51 CTH   12347   Time=3.00014x10^{-2}
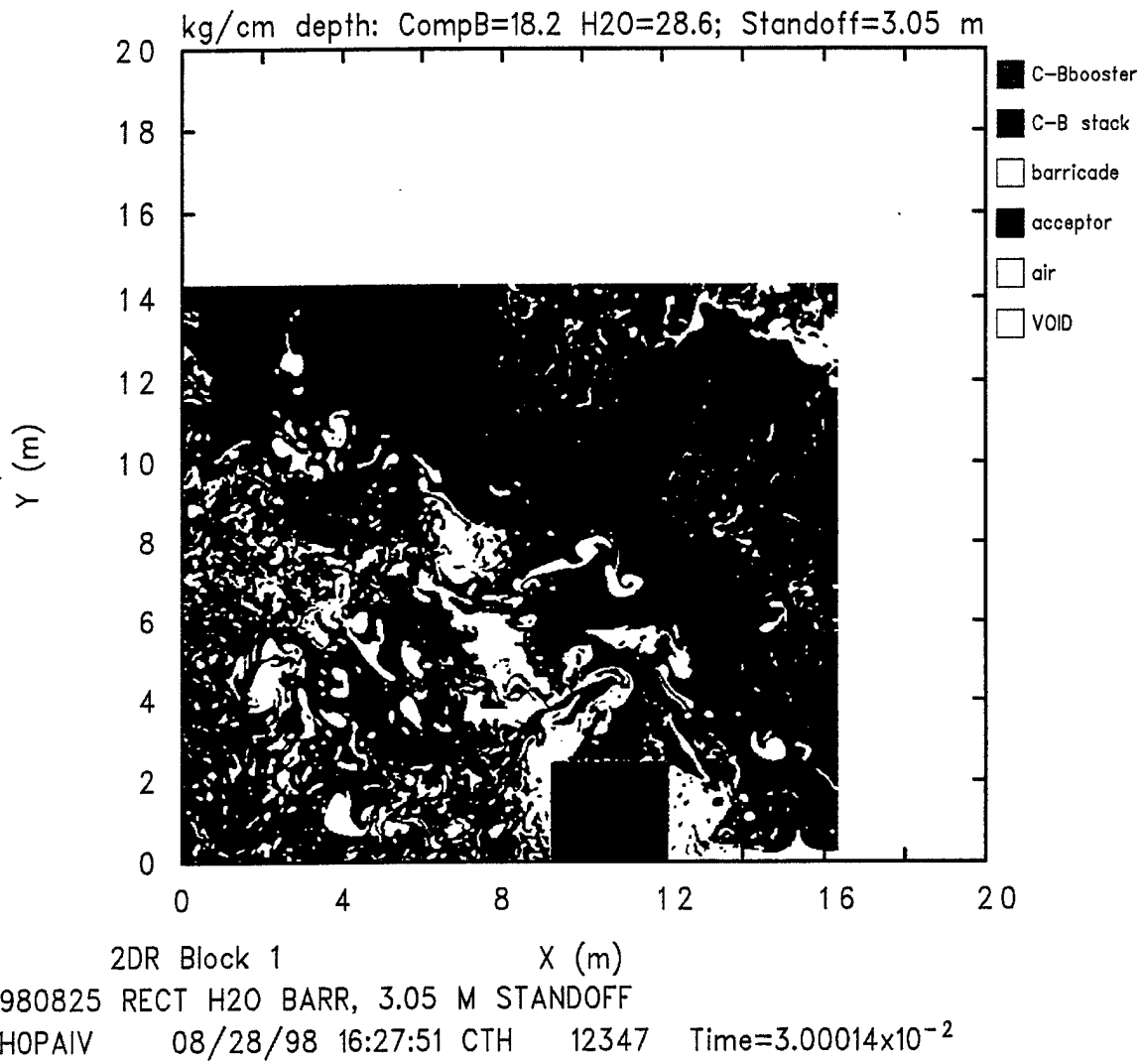
Figure 15. Flow Field at Time = 30.0 ms for Computation 980825, 3.05-m Standoff, Thin Rectangular Barricade.
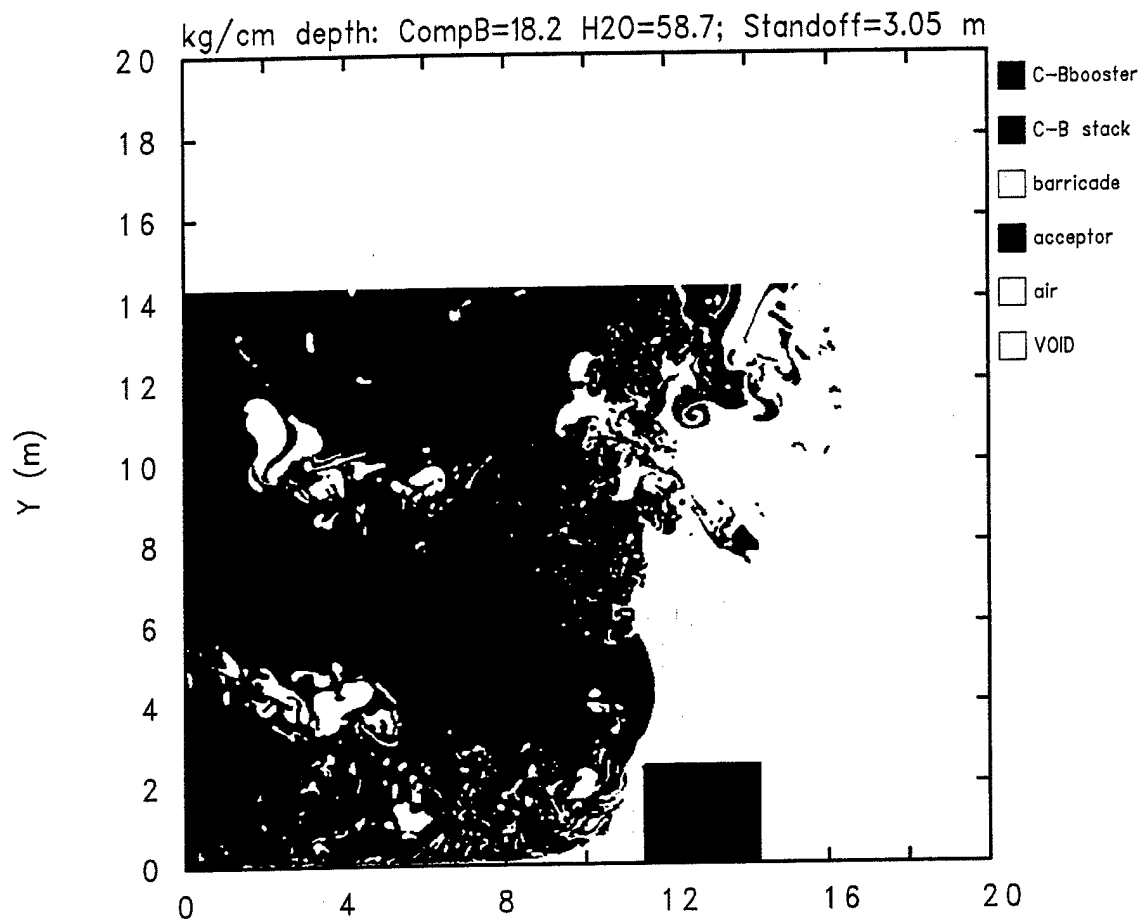
Figure 16. Flow Field at Time = 30.0 ms for Computation 980505, 3.05-m Standoff, Massive Trapezoidal Barricade.

Finally, Figure 17 shows the computational flow field for the rectangular water barricade at 40.0 ms after initiation. The acceptor stack is surrounded by, and in general contact with, explosive products. There is little water left in the computational flow field, and virtually none near the acceptor stack. Figure 18 for the trapezoidal barricade in Computation 980505 shows the water that has completed its strongest interaction with the left face of the acceptor stack (at around 32.5 ms) and is now in a rebound stage at 40.0 ms. The highly distorted barricade is still functioning as a barrier that is keeping explosive products away from the acceptor stack faces. Thus, it is readily apparent, at least from a qualitative point of view from comparing the flow fields, that the thin rectangular water barricade was considerably less capable in protecting the acceptor stack than was the more massive trapezoidal barricade. Before quantifying this statement, similar sequences of the flow fields for the thin rectangular water barricade for a 2.50-m and a 2.00-m standoff are shown. They both show similar behavior to that for 980825, so fewer snapshots in time are presented. No direct comparisons to corresponding flow fields for the trapezoidal barricade for Computations 980521 and 980610, respectively,[2] are shown.

Computation 980826 simulated a standoff distance of 2.50 m for the same thin rectangular water barricade. Figure 19 shows the computational flow field at time = 0.0. Except for the standoff distance, the computational flow field, the munitions stacks, and the barricade are identical to those for 980825 (see Figure 1).

Figure 20 shows the computational flow field at time = 5.0 ms for Computation 980521. This shows similar behavior to that shown in Figure 3 for 980825, except that the barricade is closer in space and time to its initial contact with the acceptor stack left face. Figure 21 shows the flow field at 10.0 ms after initiation. The barricade has already completed its most significant impact on the acceptor stack left face and is now rebounding from it. The barricade no longer has a recognizable rectangular shape. It is highly distorted, with what had been the upper section being dispersed into the flow field above the acceptor stack. Explosive products are approaching the top surface of the acceptor stack. Figures 22, 23, 24, and 25 show the flow field at 15.0 ms, 20.0 ms, 30.0 ms, and 40.0 ms, respectively, with the continued dispersal of the water from the barricade and increasing impingement of explosive products on various faces of the acceptor stack.

The last computation in this series, Computation 980827, simulated a standoff distance of 2.00 m. Figure 26 shows the computational flow field at time = 0.0. Except for the standoff distance, the computational flow field, the munitions stacks, and the barricade are identical to those for the Computations 980825 and 980826. A comparison with Figure 1 shows how much closer the layout of the stacks and barricade is in 980827. The bottom-left corner of the barricade is 1.048 m closer to the donor stack than in 980825, and the bottom-right corner of the barricade is similarly 1.048 m closer to the acceptor stack. Therefore, the acceptor stack in 980827 is 2.096 m closer to the donor stack than in 980825. The finite-difference grid and overall dimensions of the computational flow field, left boundary to right boundary and bottom boundary to top boundary, are identical in Computations 980825, 980826, and 980827. Figures 27, 28, 29, 30, 31, and 32 show the computational flow
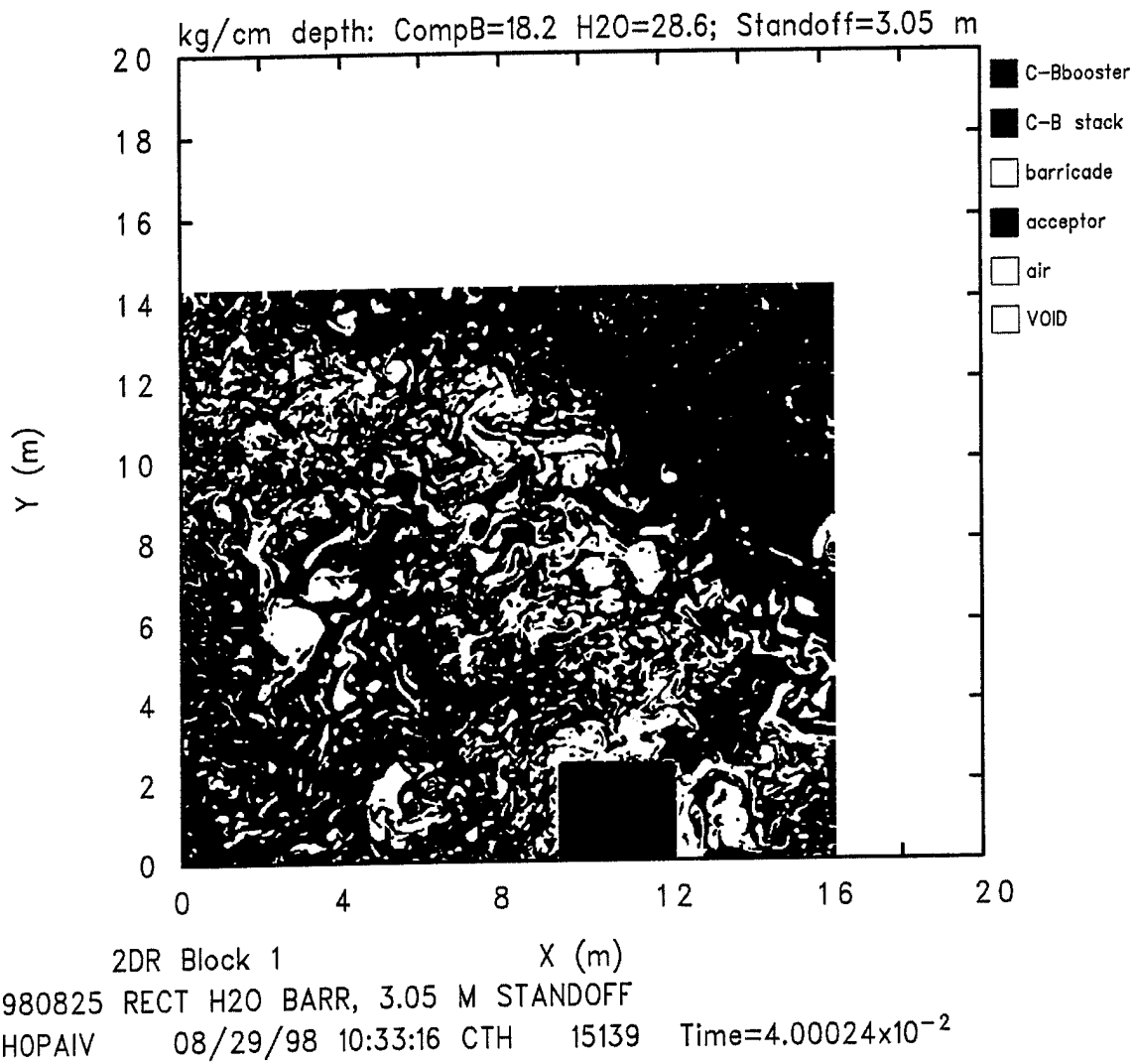
Figure 17. Flow Field at Time = 40.0 ms for Computation 980825, 3.05-m Standoff, Thin Rectangular Barricade.
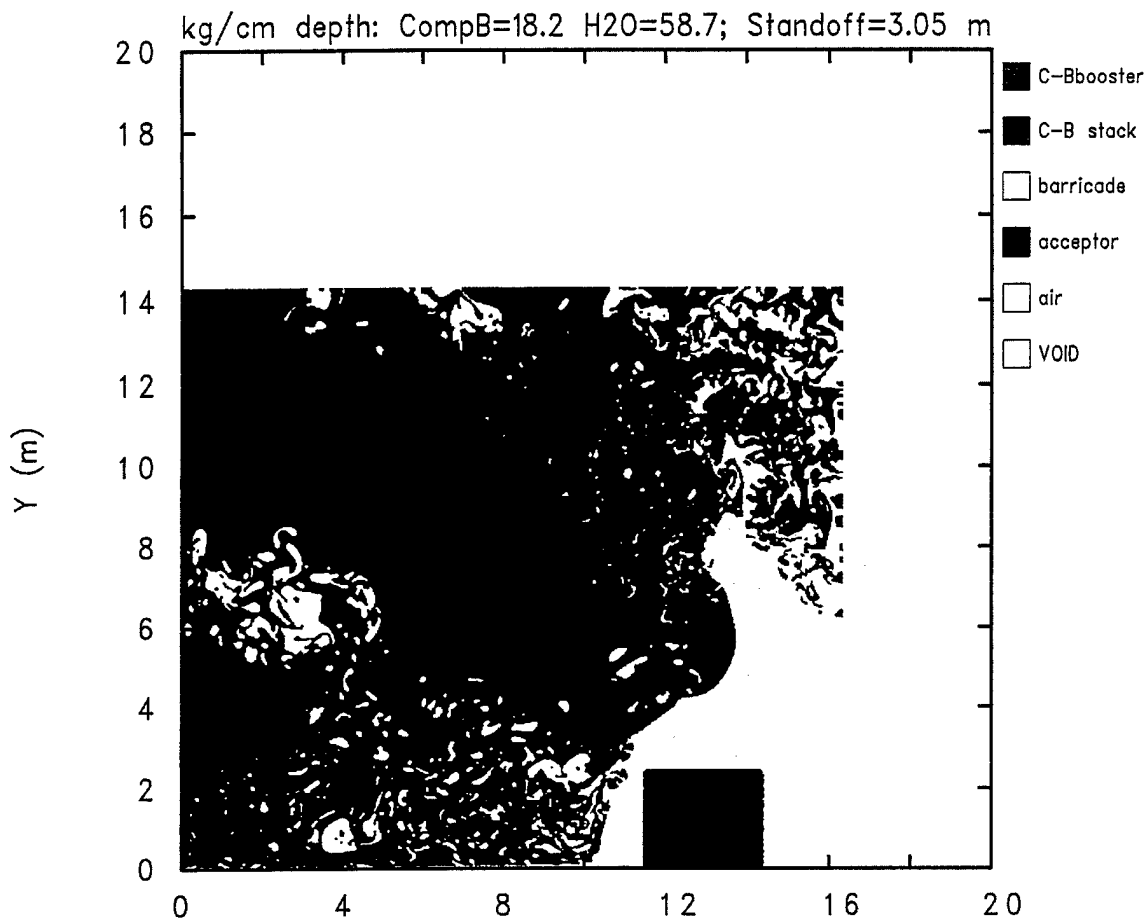
Figure 18. Flow Field at Time = 40.0 ms for Computation 980505, 3.05-m Standoff, Massive Trapezoidal Barricade.

kg/cm depth: CompB=18.2 H2O=28.6; Standoff=2.50 m
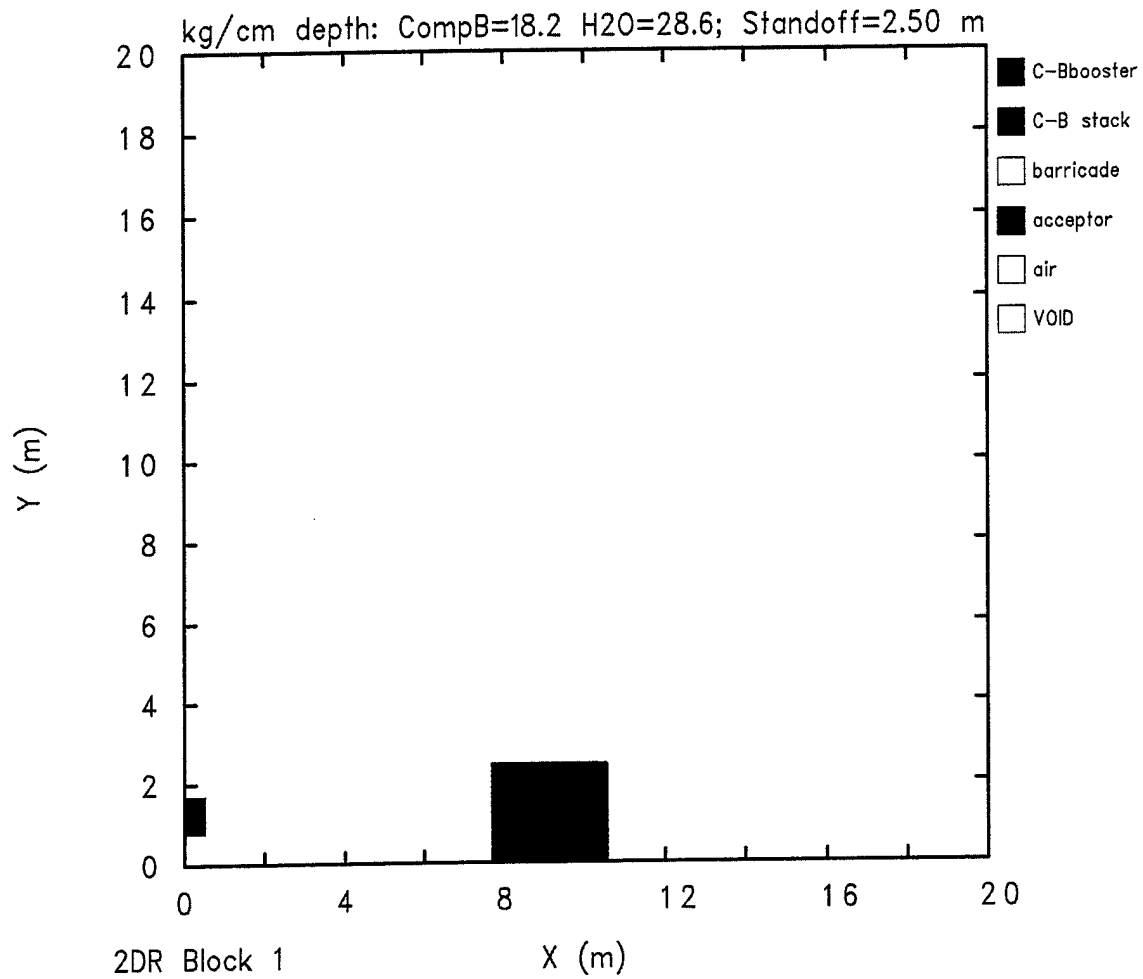
2DR Block 1

980826 RECT H2O BARR, 2.50 M STANDOFF

HZKAEF G 08/26/98 10:01:49 CTHGEN 0 Time=0.

Figure 19. Flow Field at Time = 0.0 for Computation 980826, 2.50-m Standoff, Thin Rectangular Barricade.

kg/cm depth: CompB=18.2 H2O=28.6; Standoff=2.50 m

C–Bbooster
C–B stack
barricade
acceptor
air
VOID

2DR Block 1   X (m)
980826 RECT H2O BARR, 2.50 M STANDOFF
HZKBHA   08/27/98 06:05:24 CTH   3469   Time=5.00177x10^{-3}

Figure 20. Flow Field at Time = 5.0 ms for Computation 980826, 2.50-m Standoff, Thin Rectangular Barricade.

Figure 21. Flow Field at Time = 10.0 ms for Computation 980826, 2.50-m Standoff, Thin Rectangular Barricade.

kg/cm depth: CompB=18.2 H2O=28.6; Standoff=2.50 m

2DR Block 1   X (m)
980826 RECT H2O BARR, 2.50 M STANDOFF
HOPFGU   08/28/98 10:57:46 CTH   8210   Time=1.50008x10^{-2}

Figure 22. Flow Field at Time = 15.0 ms for Computation 980826, 2.50-m Standoff, Thin Rectangular Barricade.

Figure 23. Flow Field at Time = 20.0 ms for Computation 980826, 2.50-m Standoff, Thin Rectangular Barricade.

Figure 24. Flow Field at Time = 30.0 ms for Computation 980826, 2.50-m Standoff, Thin Rectangular Barricade.

Figure 25. Flow Field at Time = 40.0 ms for Computation 980826, 2.50-m Standoff, Thin Rectangular Barricade.

field at time = 5.0 ms, 10.0 ms, 15.0 ms, 20.0 ms, 30.0 ms, and 40.0 ms, respectively, for Computation 980827. Collectively, the figures show the same qualitative behavior as those for Computations 980825 and 980826, with events happening at a faster rate with respect to time.

3.2. Barricade Dynamics

Figure 33 shows the bulk momentum per centimeter depth of the water barricade in the X direction. Positive momentum is in the direction of increasing values of X. Figure 33 includes the X-direction momentum for each of the three fully coupled computations in this series for the thin rectangular barricade, plus that for Computation 980505[2] for the massive trapezoidal barricade at a 3.05-m standoff. Hereinafter, any use of the term "momentum" or the other variables (e.g., velocity, acceleration, and displacement) derived from it should be construed as referring to the bulk value in the X direction per centimeter depth, unless specifically stated otherwise. The term "bulk" is implied but used only sparingly in order to avoid repetition. The momentum shown here is the combined momentum for all of the water in the flow field at each computational time step. Values for the mass and momentum for the water (and all other materials) are saved after each time step. During any given time step later in the computations, some water flows out of the flow field through either or both of the top and right transmissive boundaries. Each of the three curves for the thin rectangular barricade shows a very rapid, monotonic initial increase in momentum with decreasing standoff. The curve for Computation 980827 (2.00-m standoff) shows the first, very abrupt decrease in momentum after its peak at 4.5 ms, followed by 980826 (2.50-m standoff) after its peak at 5.4 ms, and then 980825 (3.05-m standoff) after its peak at 6.6 ms. This very rapid drop in each curve for the thin rectangular barricade is because of the nearly simultaneous bottom-to-top strike of the barricade on the left face of the acceptor stack. As may be seen in Figure 33, the thin rectangular barricade delivers most of its momentum to the acceptor stack over a very short period of time. The fourth curve shown in Figure 33, labeled "980505 Trap, Standoff 3.05 m," is for the momentum of the massive trapezoidal water barricade at a 3.05-m standoff.[2] It shows a more gradual increase to a considerably lower peak momentum with a two-stage, much smaller total decrease in momentum. It is interesting to point out here that, while there is not much difference in both the peak momenta and the values to which the momenta for the rectangular barricade decrease by 10 ms as a function of standoff distance, there is a great difference in both peak momentum and change in momentum that can be seen when comparing the thin rectangular barricade with the massive trapezoidal barricade at the same 3.05-m standoff distance. Table 1 contains a summary of several X-direction parameters that describe some of the bulk motion of the barricade for the various computations. First among those parameters, after the computation numbers and standoff distances, are the peak X-direction bulk-momentum values for the barricade, along with their respective times of occurrence, listed with more significant figures than were typically used in the text for completeness. In order to facilitate comparisons,

34

kg/cm depth: CompB=18.2 H2O=28.6; Standoff=2.00 m

Legend:
- C-Bbooster
- C-B stack
- barricade
- acceptor
- air
- VOID

Y (m) axis: 0, 2, 4, 6, 8, 10, 12, 14, 16, 18, 20

X (m) axis: 0, 4, 8, 12, 16, 20

2DR Block 1

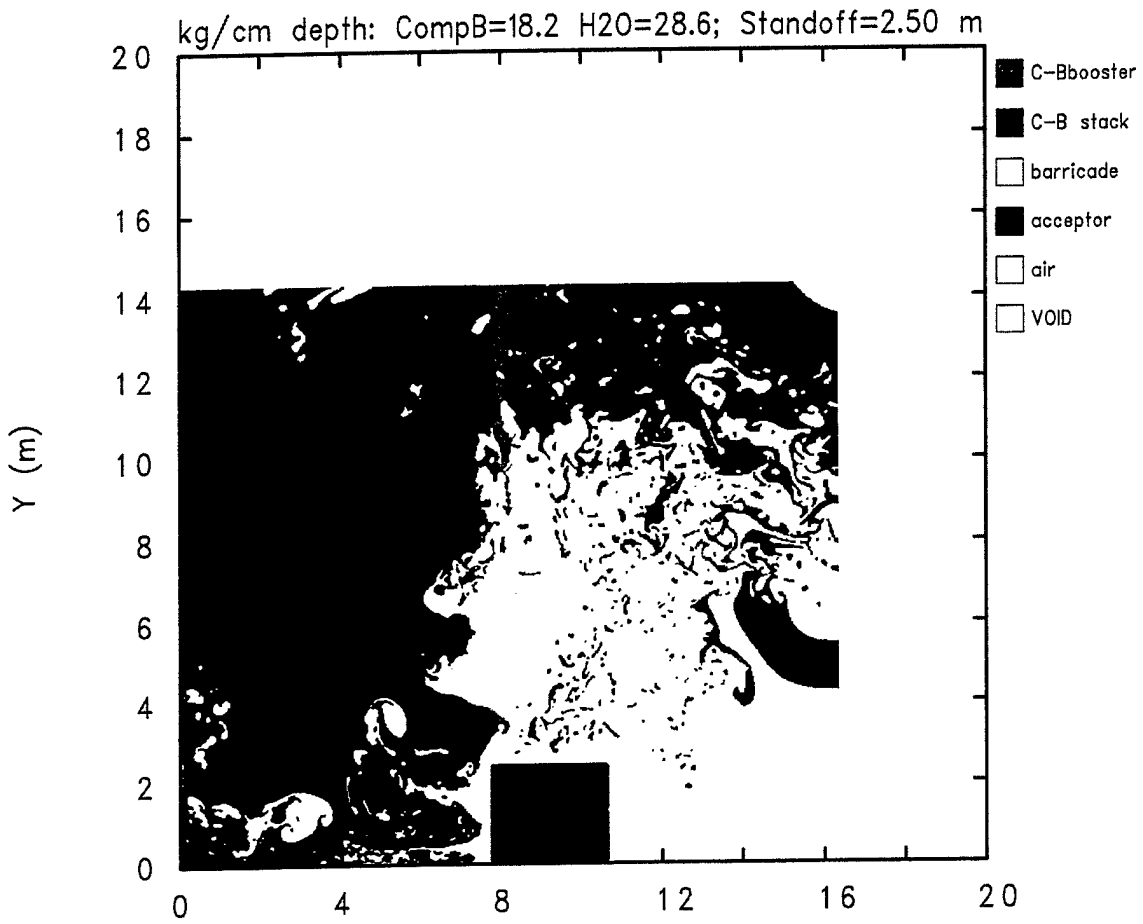980827 RECT H2O BARR, 2.00 M STANDOFF

HZMCVG G   08/26/98 12:31:44 CTHGEN   0   Time=0.
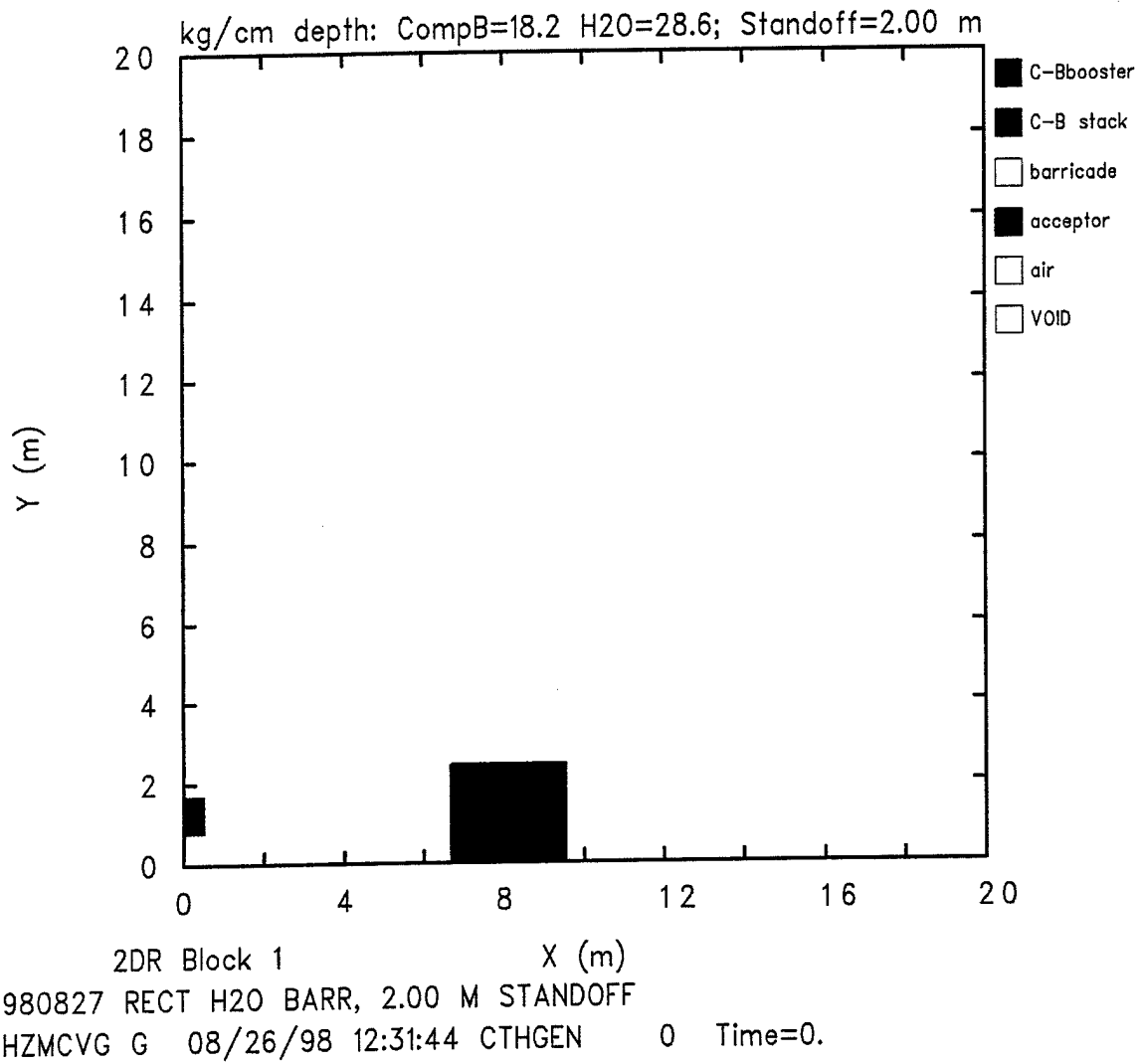
Figure 26. Flow Field at Time = 0.0 for Computation 980827, 2.00-m Standoff, Thin Rectangular Barricade.

Figure 27. Flow Field at Time = 5.0 ms for Computation 980827, 2.00-m Standoff, Thin Rectangular Barricade.

Figure 28. Flow Field at Time = 10.0 ms for Computation 980827, 2.00-m Standoff, Thin Rectangular Barricade.
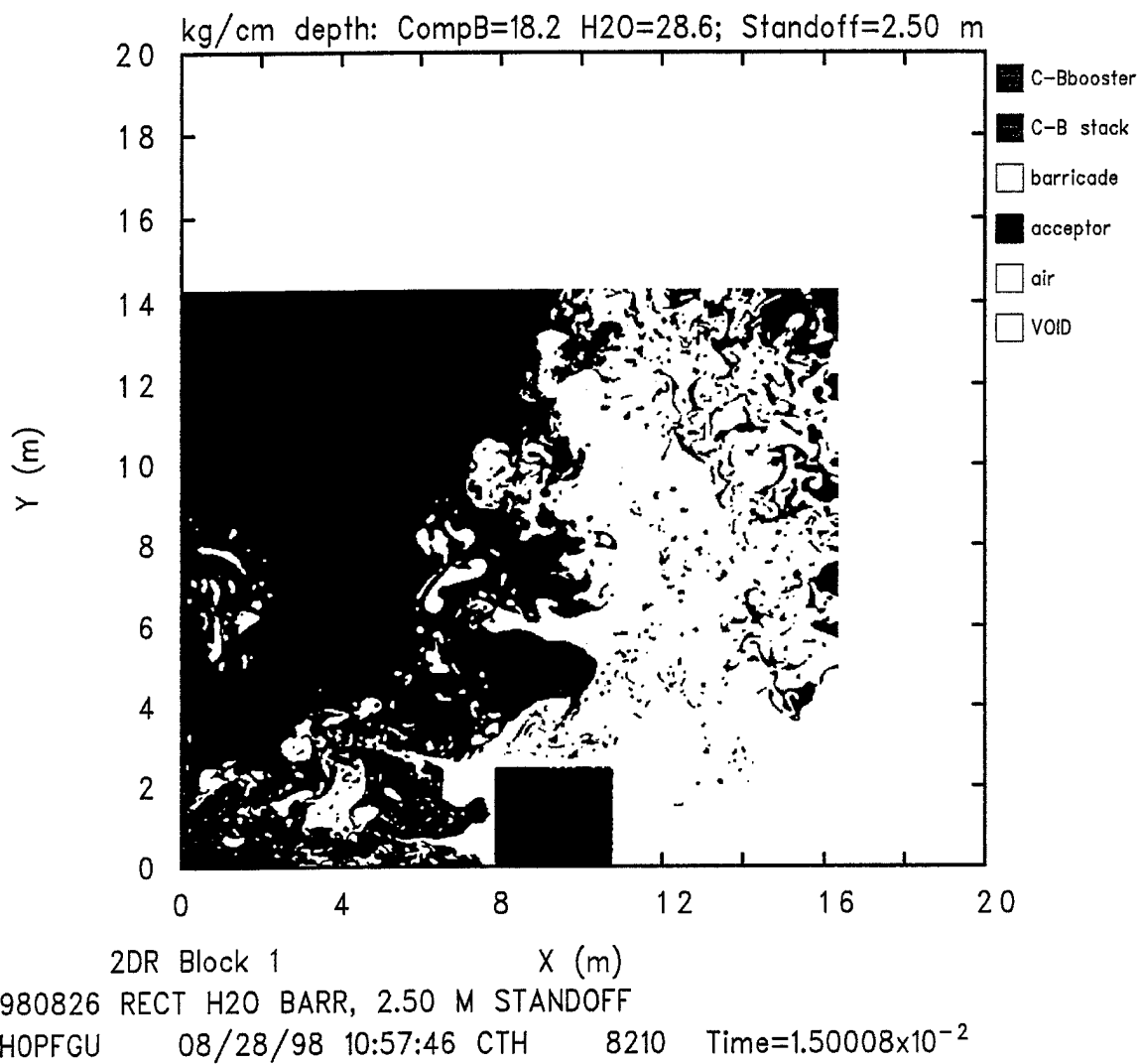
Figure 29. Flow Field at Time = 15.0 ms for Computation 980827, 2.00-m Standoff, Thin Rectangular Barricade.
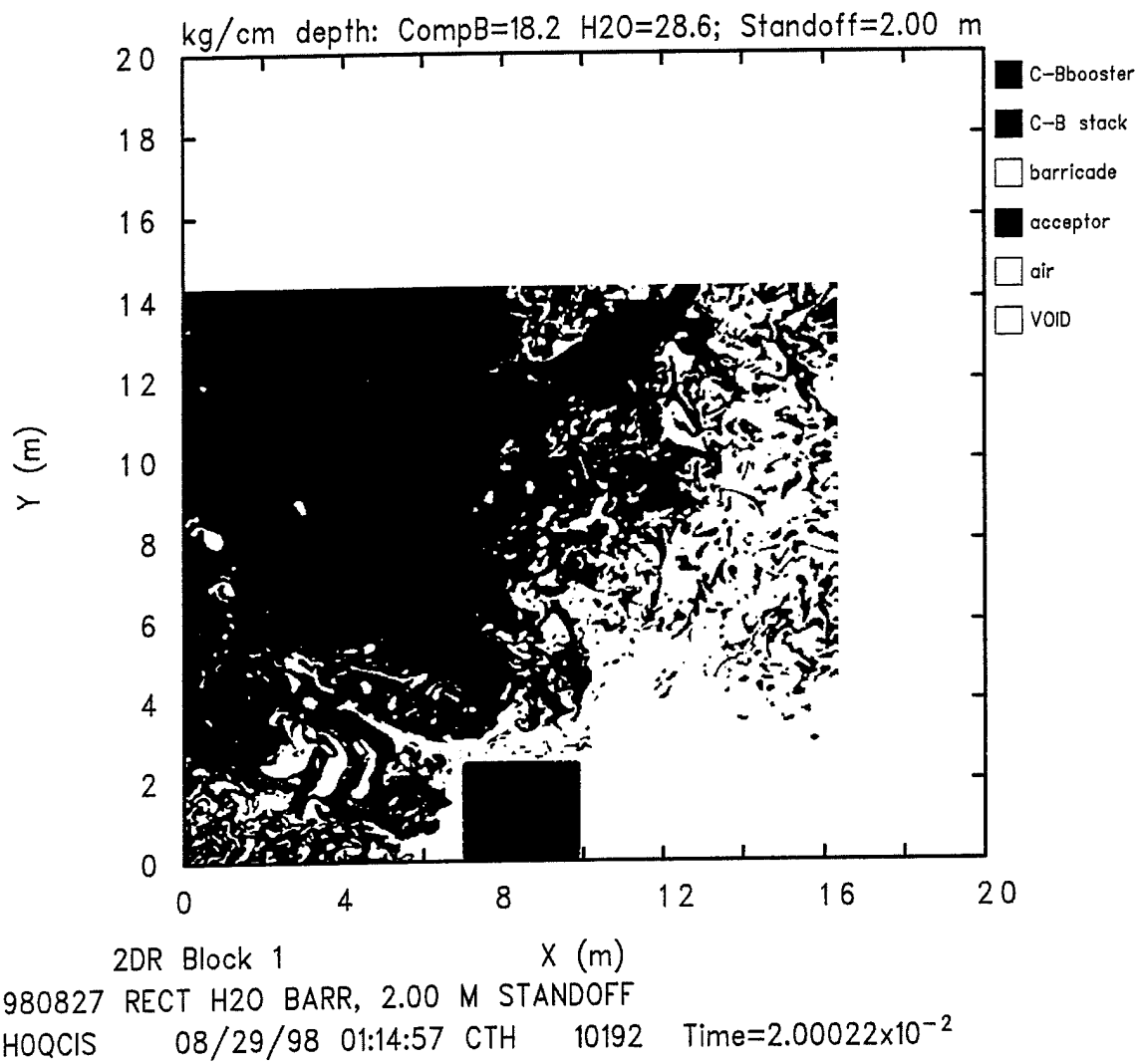
Figure 30. Flow Field at Time = 20.0 ms for Computation 980827, 2.00-m Standoff, Thin Rectangular Barricade.

Figure 31. Flow Field at Time = 30.0 ms for Computation 980827, 2.00-m Standoff, Thin Rectangular Barricade.
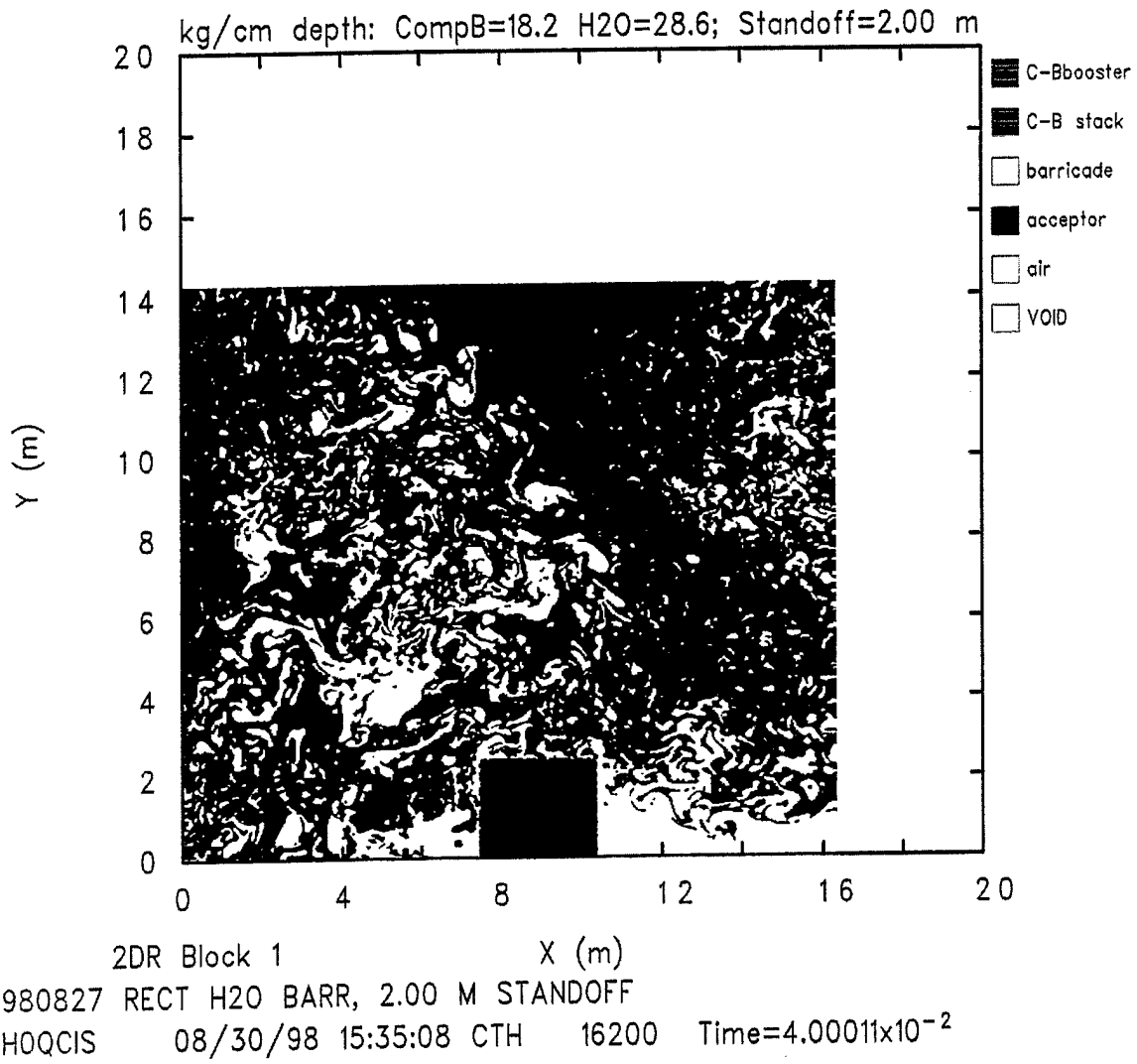
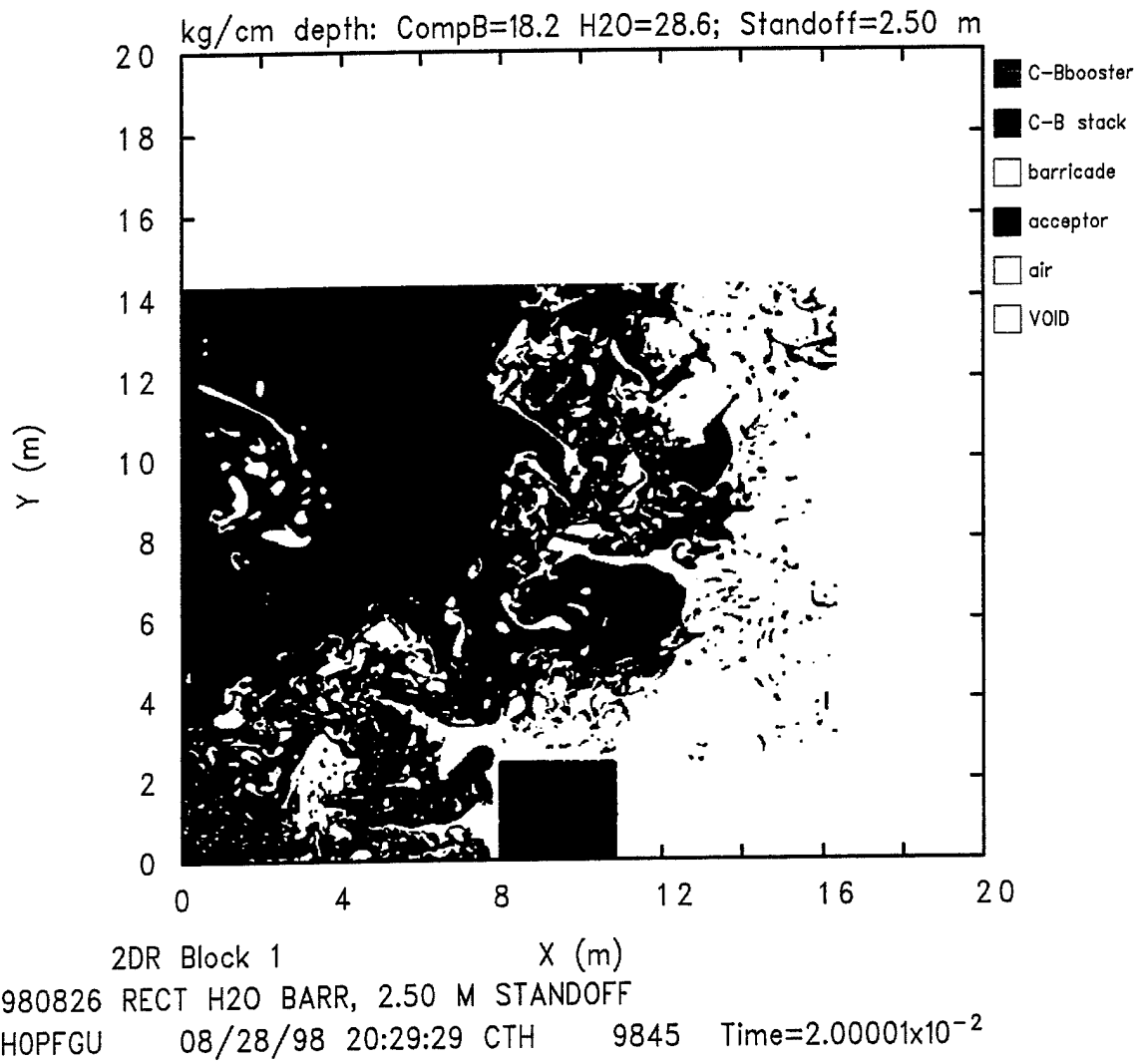Figure 32. Flow Field at Time = 40.0 ms for Computation 980827, 2.00-m Standoff, Thin Rectangular Barricade.
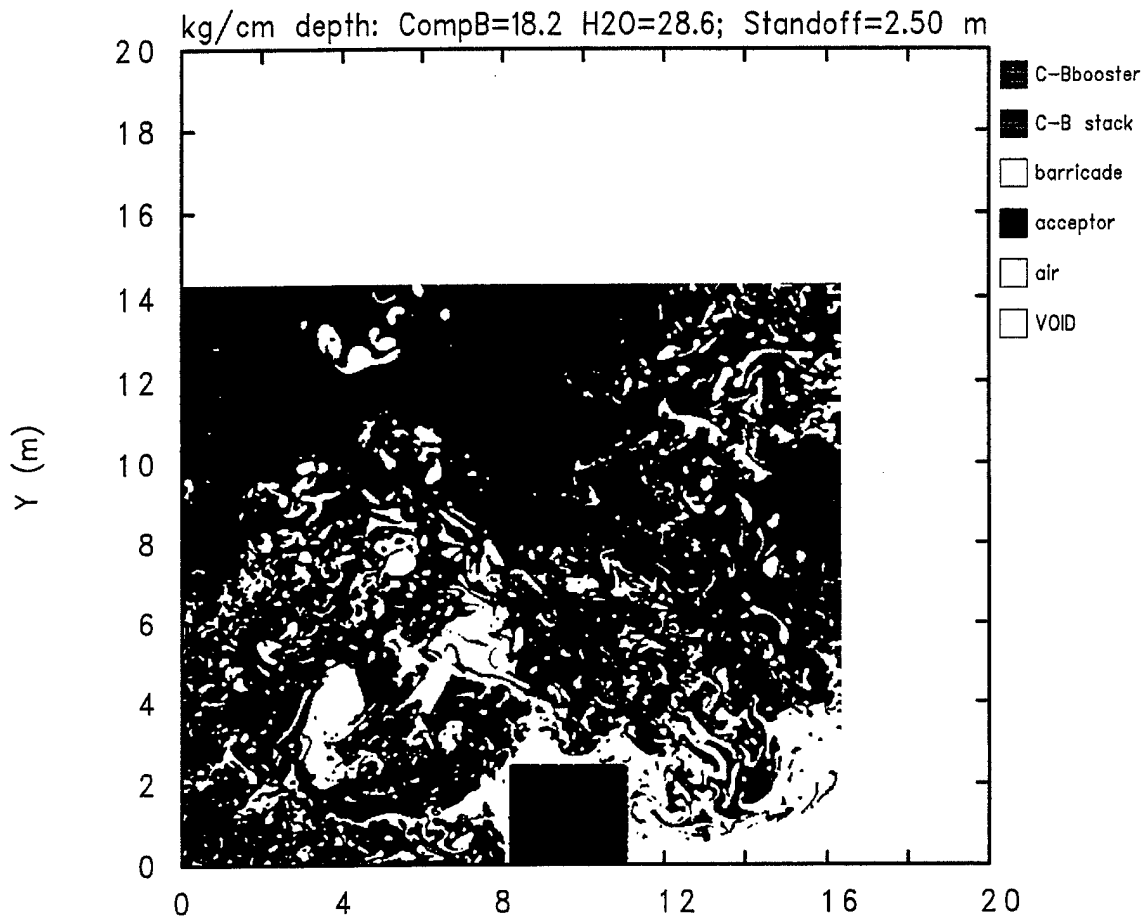
the first column of numbers is for the massive trapezoidal barricade at a 3.05-m standoff, followed by data for the thin rectangular barricade. The rest of the parameters in the table are discussed in the following paragraphs.
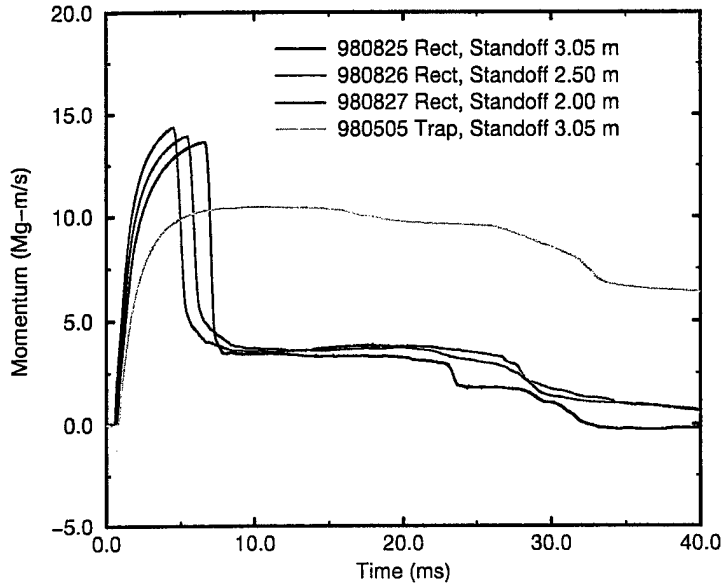
Figure 33. Water Barricade X-Direction Momentum Toward Acceptor Stack, Computations 980825 Through 980827 (Rectangular), Plus 980505 (Trapezoidal).

After each computational time step, both the total momentum and mass of the water in the flow field are known. The X-direction bulk velocity (hereinafter referred to as "X-direction velocity") of the barricade may be computed for each time step by dividing the instantaneous momentum by the corresponding mass. The X-direction velocity of the water barricade toward the acceptor stack for each standoff for the thin rectangular barricade, plus the velocity for the trapezoidal barricade at 3.05-m standoff, is shown in Figure 34. These curves are essentially scaled variants of the momentum curves shown in Figure 33 and therefore show the same relative behavior described for the momenta. The peak X-direction velocity for the thin rectangular barricade at each standoff distance is 476.6 m/s at 6.56 ms (3.05-m standoff), 486.9 m/s at 5.39 ms (2.50-m standoff), and 503.2 m/s at 4.50 ms (2.00-m standoff). For comparison, the curve for the trapezoidal barricade, labelled "980505 Trap, Standoff 3.05 m" is included in Figure 34. It has a peak velocity of 178.2 m/s at 10.9 ms, much lower than the 476.6 m/s peak for the thin rectangular barricade at the same defined standoff. The X-direction velocities become less meaningful at late time as far as the acceptor stack is concerned because of the increasing proportion of water that is in the air above the plane of the top face of the acceptor stack.

42

Table 1. Barricade Peak X-Direction Bulk-Motion Parameters.

Computation Number	Trapezoidal 980505	Rectangular 980825	Rectangular 980826	Rectangular 980827
Standoff (m)	3.048	3.048	2.50	2.00
Peak Momentum (Mg-m/s)	10.46	13.64	13.93	14.40
Time (ms)	10.07	6.560	5.388	4.500
Peak Velocity (m/s)	178.2	476.6	486.9	503.2
Time (ms)	10.93	6.560	5.388	4.500
Peak Acceleration (km/s/s)	143.4	631.5	658.0	679.7
Time (ms)	10.04	0.8141	0.6947	0.5947
Peak Left-Surface Impulse (MN-s/m)	0.9016	1.185	1.283	1.360
Time (ms)	34.48	38.29	38.54	38.85
Distance Traveled (m)	5.979	(Rebounded) 4.853	5.669	5.373
Time (ms)	39.99	32.46	39.99	39.99

Figure 34. Water Barricade X-Direction Velocity Toward the Acceptor Stack, Computations 980825 Through 980827 (Rectangular), Plus 980505 (Trapezoidal).

43

The momentum curves in Figure 33, and hence the velocity curves in Figure 34, are relatively smooth functions with respect to time. The velocities were piecewise differentiated with respect to time, using the difference values of velocity and time in the data file, to produce the curves of bulk X-direction acceleration for each standoff as shown in Figure 35. The peak positive accelerations for the thin rectangular barricade are 631.5 km/s^2 at 0.81 ms (3.05-m standoff), 658.0 km/s^2 at 0.69 ms (2.50-m standoff), and 679.7 km/s^2 at 0.59 ms (2.00-m standoff). The peak negative accelerations for the thin rectangular barricade are minus 808.7 km/s^2 at 7.09 ms (3.05-m standoff), minus 586.9 km/s^2 at 5.88 ms (2.50-m standoff), and minus 583.8 km/s^2 at 5.05 ms (2.00-m standoff). These compare with the peak positive acceleration of 143.4 km/s^2 at 1.0 ms and a peak negative acceleration of minus 19.2 km/s^2 at 32.80 ms for the massive trapezoidal barricade at a 3.05-m standoff. Because the full simulation time is displayed on the abscissa, the initial accelerations of the barricade for each standoff for the rectangular barricade appear to nearly overlay one another. Figure 36 shows a temporally expanded plot of the first 10.0 ms of the X-direction acceleration of the barricade for each computation. The initial accelerations for the rectangular barricade occur in a direct sequence based on standoff distance, with the initial acceleration for the trapezoidal barricade at a 3.05-m standoff beginning at about the same time as that for the rectangular barricade at that same standoff. The deceleration sequence for the rectangular barricade also occurs in direct correspondence to the standoff distance. No meaningful deceleration of the trapezoidal barricade occurs during the first 10.0 ms.

Figure 35. Water Barricade X-Direction Acceleration Toward the Acceptor Stack, Computations 980825 Through 980827 (Rectangular), Plus 980505 (Trapezoidal).

44
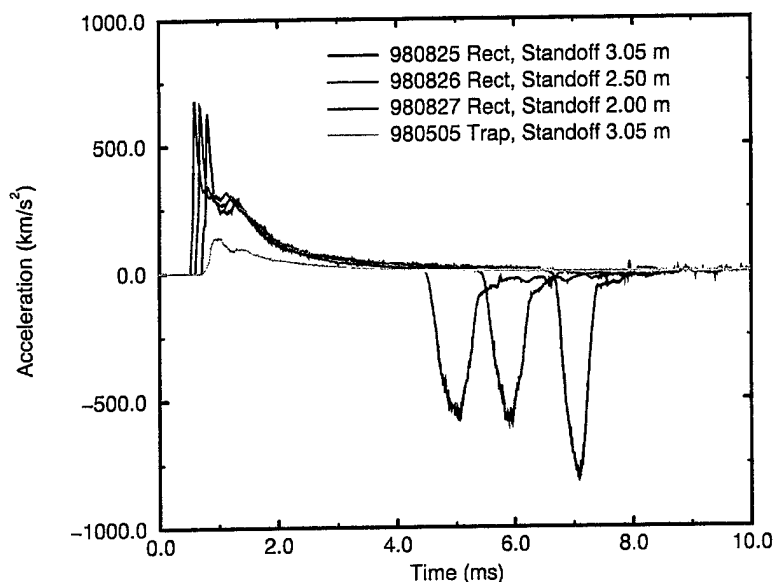
Figure 36. Water Barricade Initial X-Direction Acceleration Toward the Acceptor Stack, Computations 980825 Through 980827 (Rectangular), Plus 980505 (Trapezoidal).

Figure 37 shows the total X-direction impulse per meter depth on the left surface of the barricade. This was computed by integrating the overpressure over space and time using 30 tracer particles that were placed along the left surface of the barricade at time zero, the grid generation time. The overpressure is the absolute pressure minus the ambient atmospheric pressure. The tracer particles were allowed to move freely with the flow in the grid. As the simulated time in the computations progressed, the left surface of the barricade became increasingly distorted to the point that it was no longer clearly definable as a simple surface. Correspondingly, the impulse integral itself probably lost meaning after about 10 ms. Essentially all of the impulse from the detonation of the donor stack is delivered to the barricade in the first few milliseconds. There is a moderate inverse functional relation in impulse delivered to the rectangular barricade with respect to standoff distance, and a significant difference in the impulse delivered to the left surface of the trapezoidal barricade versus the rectangular barricade at a 3.05-m standoff distance. The peak values for the rectangular barricade are 1.185 MN-s/m at 38.3 ms (3.05-m standoff), 1.283 MN-s/m at 38.5 ms (2.50-m standoff), and 1.360 MN-s/m at 38.8 ms (2.00-m standoff). Because of the surface distortion just discussed, the times of these peaks are not particularly important and are included only for completeness. This equates to a direct ratio of peak impulse of 1.148 for an inverse ratio in relative standoff distance of 1.524 for the standoff range of 3.05 m to 2.00 m, somewhat greater than the impulse ratio of 1.068 reported earlier[2] for the trapezoidal barricade. The peak for the trapezoidal barricade at the 3.05-m standoff is 0.9016 MN-s/m

45

at 34.5 ms, which is 23.9 percent below that for the rectangular barricade at the same standoff.
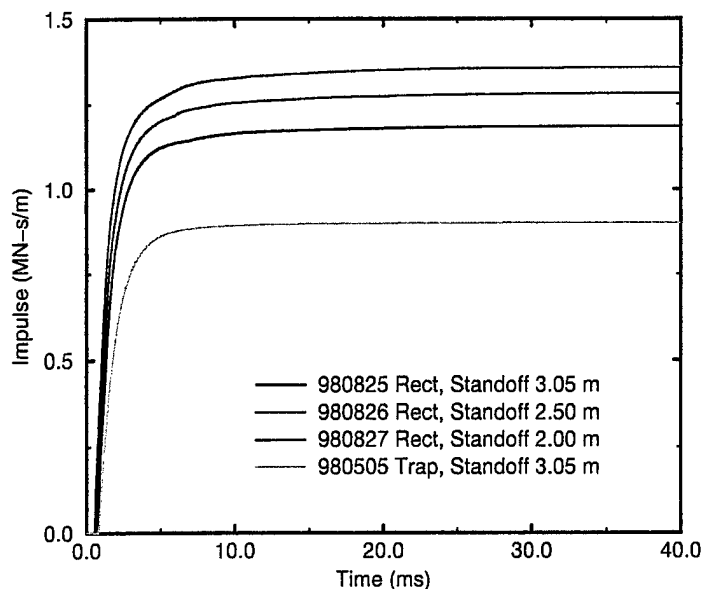
Figure 37. Water Barricade Left Surface Total X-Direction Impulse per Meter Depth, Computations 980825 Through 980827 (Rectangular), Plus 980505 (Trapezoidal).

The velocity data are used to compute the bulk translation of the barricade versus time, which is shown in Figure 38. The curves for the rectangular barricade are most meaningful through about 6 ms. At about this time the barricade impacts the acceptor stack. The peak distance of 4.853 m for 980825 occurs at what seems to be an early time of 32.46 ms because of a pronounced net rebound of a part of the barricade from the acceptor stack left surface. The curve for the displacement of the barricade in Computation 980505 shows less displacement through about 30 ms.

Figure 39 shows the functional relations of the peak values (at different times) of the several parameters just described for the barricade in the preceding figures. The abscissa shows the dimensional standoff distance. The ordinate shows the normalized direct ratio of parameters, the value of a given parameter at a given standoff divided by the corresponding value for the 3.048-m standoff. The curves for the peak momentum and the peak velocity overlay one another because of the direct scaling by mass between them. Therefore, the red curve for the peak velocity is plotted as a dashed line overwritten upon the solid black line for the peak momentum. This gives the appearance of a dashed black line in the plot itself for what is actually a solid black line. Figure 40 shows the same data as in Figure 39, but with the abscissa showing the normalized inverse standoff ratio, computed as 3.048 m divided by each successive standoff ratio. Thus, the value for the 3.048-m standoff itself is
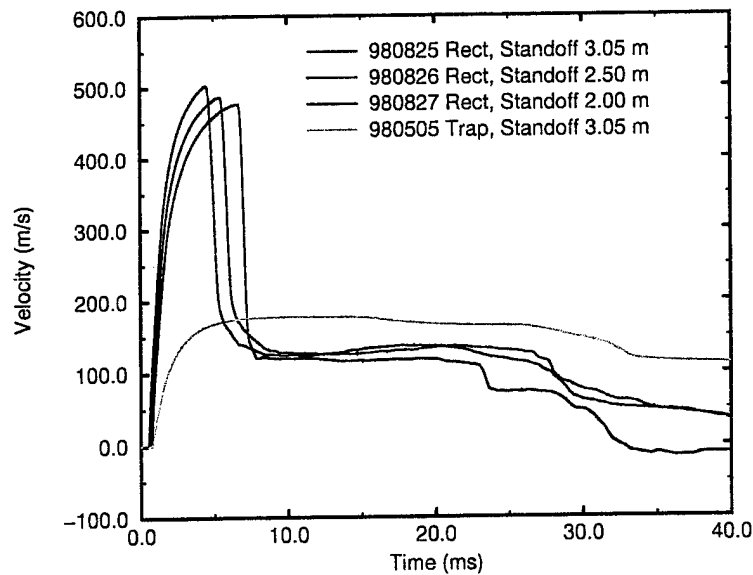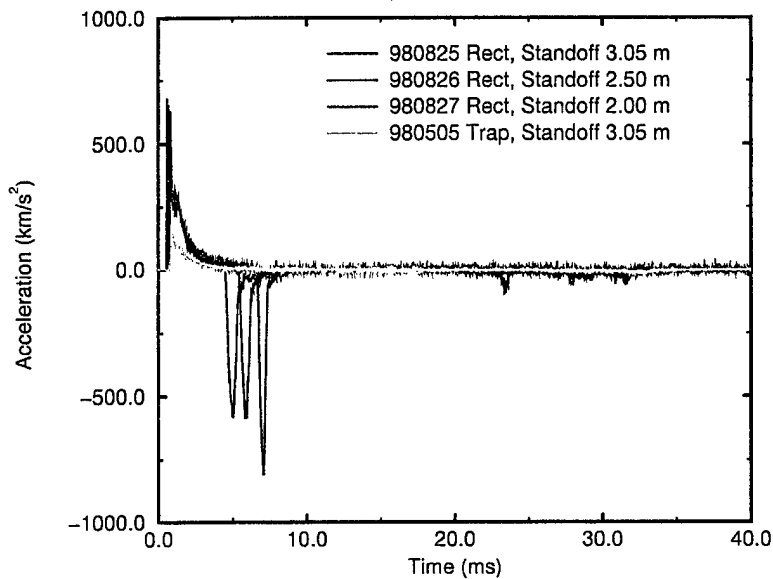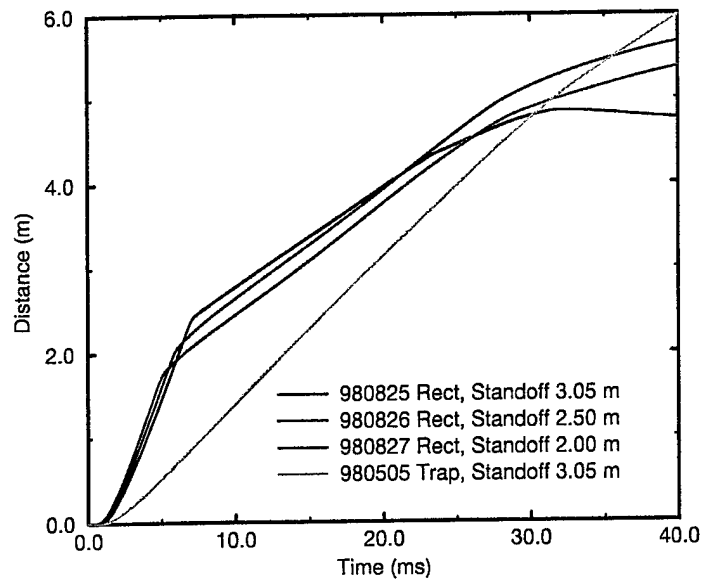
Figure 38. Water Barricade X-Direction Distance Moved Toward the Acceptor Stack, Computations 980825 Through 980827 (Rectangular), Plus 980505 (Trapezoidal).

1.0, and the value for the 2.00-m standoff is 1.524. The ordinate is the same as for Figure 39 except for its scaling. The abscissa and ordinate scales are forced to be equal so that any $\Delta X/\Delta Y = \pm 1.0$ relationship would show as a ± 45-degree straight line. The figures show a weak functional relation of all of these normalized parameters with both dimensional and normalized standoff. This shows that, as far as these parameters for this simplified barricade are concerned, there is only a minor penalty in barricade whole-body dynamics incurred by moving the barricade closer to the donor stack to a nominal 2-m from a nominal 3-m standoff. Figure 41 shows the same data as in Figure 40, but with the abscissa and ordinate forced to a scaling that will facilitate comparison with similar data for the acceptor stack shown later in the next section. While this forced scaling produces what appears to be an excess amount of "white space" in the plot, its value for the later comparison exceeds the apparent lack of esthetics.

3.3. Acceptor Stack Dynamics

Figure 42 shows the bulk momentum per centimeter of depth of the acceptor stack in the X direction for the three computations with the thin rectangular barricade. Included in that figure is the bulk momentum per centimeter depth of the acceptor stack from the 3.05-m standoff computation, 980505, with the massive trapezoidal water barricade.[2] Positive momentum is defined in the positive X direction as before. There is only a minimal

47
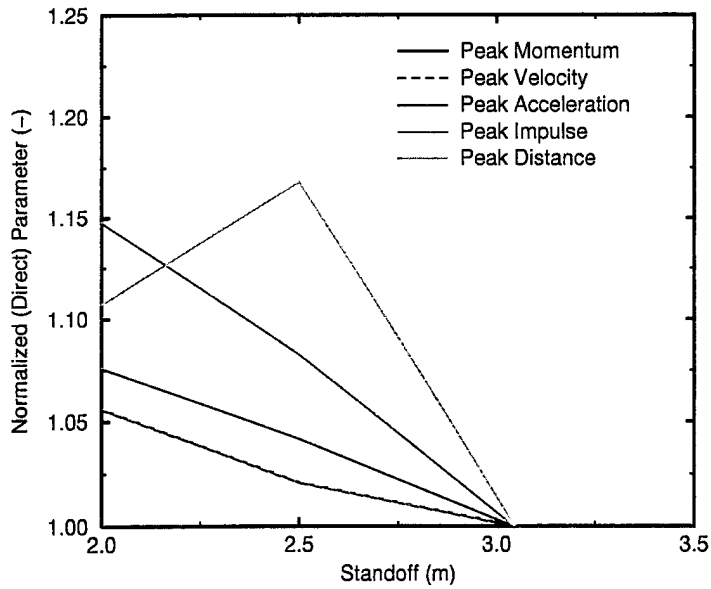
Figure 39. Normalized (Direct Ratio) Barricade Parameters Versus Standoff Distance, Computations 980825 Through 980827.
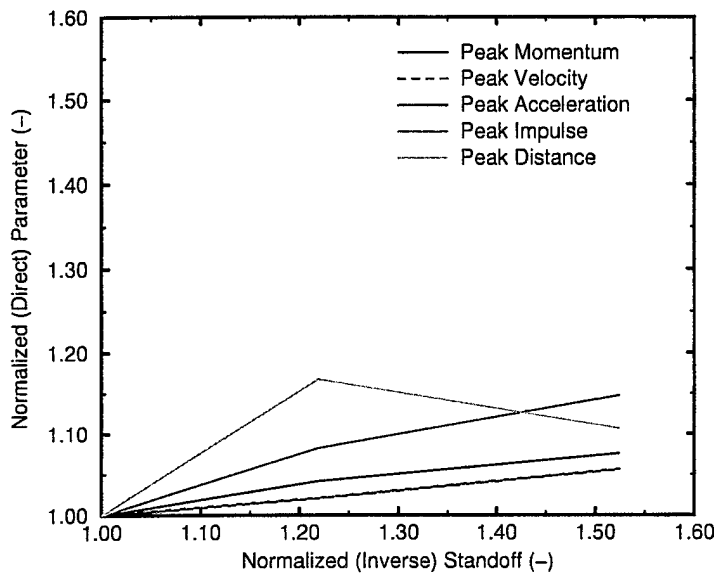
Figure 40. Normalized (Direct Ratio) Barricade Parameters Versus Normalized (Indirect Ratio) Standoff Distance, Computations 980825 Through 980827.

48
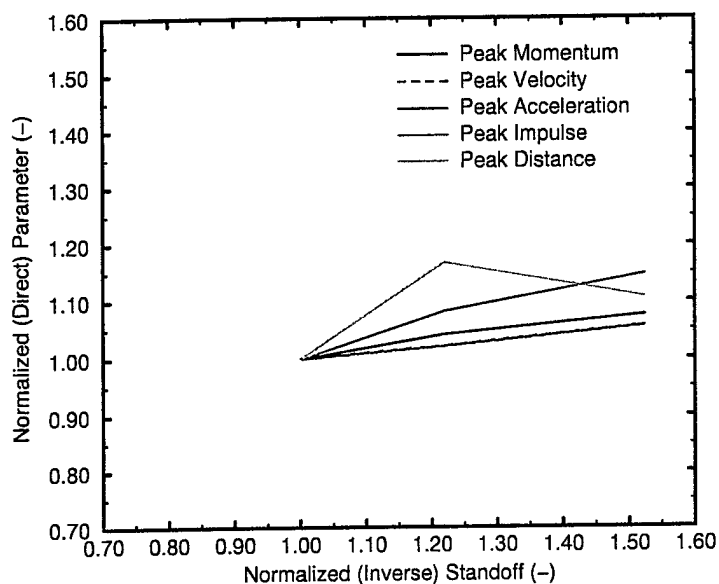
Figure 41. Normalized (Direct Ratio) Barricade Parameters Versus Normalized (Indirect Ratio) Standoff Distance (Rescaled), Computations 980825 Through 980827.

increase in the momentum of the acceptor stack caused by the air shock for the three thin rectangular barricade computations. After about 5 ms, all three computations show a very rapid increase in momentum caused by the impact of the water barricade. The acceptor stack momentum from the 3.05-m standoff computation for the massive trapezoidal water barricade shows the three-stage sequential increase in momentum described previously[2] that is caused by the air shock, the impact of the water wave on the top-left surface of the acceptor stack, and then the impact of the lower sections of the barricade on the acceptor stack. The momentum of the acceptor stack at 40.0 ms for Computation 980825 (rectangular barricade, 3.05-m standoff, 28.61 kg/cm of depth) is 11.90 Mg-m/s, which is 3.00 times the corresponding value of 3.962 Mg-m/s for Computation 980505 (trapezoidal barricade, 3.05-m standoff, 58.71 kg/cm of depth). The final momentum values at 40.0 ms are 12.01 Mg-m/s for the 2.50-m standoff and 12.95 Mg-m/s for the 2.00-m standoff. Table 2 contains a summary of several X-direction parameters that describe some of the bulk motion of the acceptor stack for the various computations. First among those parameters, after the computation numbers and standoff distances, are the peak X-direction bulk-momentum values for the acceptor stack, along with their respective times of occurrence, listed with more significant figures than were typically used in the text for completeness. In order to facilitate comparisons, the first column of numbers is for the acceptor stack in Computation 980505 with the massive trapezoidal barricade at a 3.05-m standoff, followed by columns of data for the thin rectangular barricade computations. The rest of the parameters in the table are discussed in the following paragraphs.

49

Figure 42. Acceptor Stack X-Direction Momentum for Computations 980825 Through 980827 (Rectangular), Plus 980505 (Trapezoidal).

Table 2. Acceptor Stack Peak X-Direction Bulk-Motion Parameters.

Computation Number	Trapezoidal 980505	Rectangular 980825	Rectangular 980826	Rectangular 980827
Standoff (m)	3.048	3.048	2.50	2.00
Peak Momentum				
(Mg-m/s)	3.962	11.90	12.01	12.95
Time (ms)	40.00	39.87	39.88	38.99
Peak Velocity				
(m/s)	33.40	100.3	101.2	109.2
Time (ms)	40.00	39.87	39.88	38.99
Peak Acceleration				
(km/s/s)	9.277	197.5	144.8	142.8
Time (ms)	32.80	7.093	5.965	5.024
Peak Left-Surface Impulse				
(MN-s/m)	0.3725	1.138	1.154	1.248
Time (ms)	39.99	39.99	39.99	39.99
Distance Traveled				
(m)	0.4065	3.237	3.360	3.718
Time (ms)	39.99	39.99	39.99	39.99

50

The corrected mass of the acceptor stack was used to compute the bulk X-direction velocity from the momentum of the acceptor stack. The results are shown in Figure 43. The curves show the same timing and differentiation as those for the acceptor stack momentum. The velocities of the acceptor stack at 40.0 ms for the thin rectangular barricade are 100.3 m/s (3.05-m standoff), 101.2 m/s (2.50-m standoff), and 109.2 m/s (2.00 m standoff). The velocity of the acceptor stack for the massive trapezoidal water barricade at a 3.05-m standoff, also shown in Figure 43, is 33.4 m/s.

Figure 43. Acceptor Stack X-Direction Velocity, Computations 980825 Through 980827 (Rectangular), Plus 980505 (Trapezoidal).

As was done for the barricade, the acceptor stack velocity for each standoff was piecewise differentiated with respect to time to compute the bulk X-direction acceleration of the acceptor stack. The acceleration curves for the three thin rectangular barricade computations and Computation 980505 are shown in Figure 44. Each individual curve for the rectangular barricade shows a single, large spike in acceleration in the order of increasing standoff distance. All occur before 10 ms. Interestingly, the greatest peak of the three is 197.5 km/s^2 for the 3.05-m standoff. This is far greater than the 9.28 km/s^2 for the trapezoidal barricade at a 3.05-m standoff, which occurs at 32.8 ms.

The acceptor stack was modeled as a solid iron rectangle so that the most reliable loading possible could be computed for its left face. Thirty tracer particles were uniformly spaced along the left face, top to bottom, of the acceptor stack. They were constrained from moving in either the X or Y direction so that the ensuing hydrodynamic flows would not sweep them off the face of the acceptor stack or reposition them horizontally or vertically.

Figure 44. Acceptor Stack X-Direction Acceleration for Computations 980825 Through 980827 (Rectangular), Plus 980505 (Trapezoidal).

The overpressure histories were integrated over space and time to compute the total X-impulse per meter depth versus time for each standoff. These curves are shown in Figure 45. The acceptor stack shows that the thin rectangular water barricade provided a very efficient delivery of its left-face impulse from the blast loading caused by the detonation of the donor stack (see Figure 37) to the acceptor stack at its right face. The acceptor stack left-face values are nearly equal to the respective barricade left-face values. The final impulse values per meter depth on the acceptor stack left face are 1.138 MN-s/m (3.05-m standoff), a minimally higher value of 1.154 MN-s/m (2.50-m standoff), and 1.248 MN-s/m (2.00-m standoff). In Computation 980505 for the trapezoidal barricade, the final impulse per meter depth is 0.3725 MN-s/m (3.05-m standoff), which is 0.327 times that for the 3.05-m standoff rectangular barricade, and 0.413 times the 0.9016 MN-s/m impulse on the left side of the trapezoidal barricade.

Figure 46 shows the distance that the acceptor stack moves as a result of the blast and impact loading by 40.0 ms. The range for Computations 980825 through 980827 for the rectangular barricades is from 3.24 m (3.05-m standoff) to 3.72 m (2.00-m standoff). In Computation 980505 for the trapezoidal barricade, the acceptor stack moves 0.41 m in 40.0 ms, 12.6 percent that for the acceptor stack in Computation 980825 for the rectangular barricade at a 3.05-m standoff.

Figure 47 shows the functional relations of the peak (at different times) and final (at 40.0 ms) values of the several parameters versus standoff distance that were just described
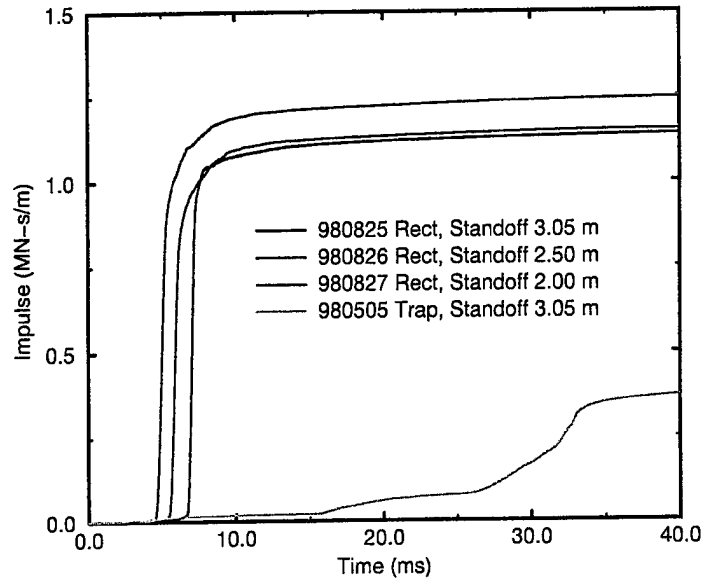
Figure 45. Acceptor Stack X-Direction Total Impulse per Meter Depth, Computations 980825 Through 980827 (Rectangular), Plus 980505 (Trapezoidal).
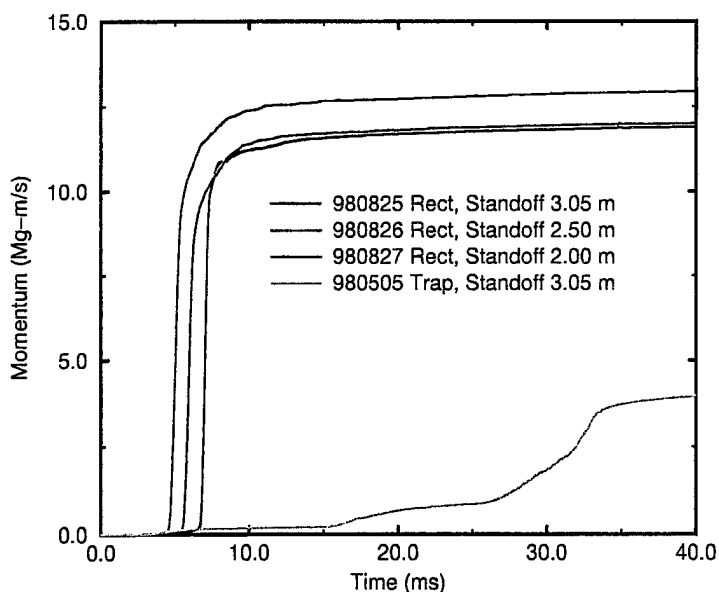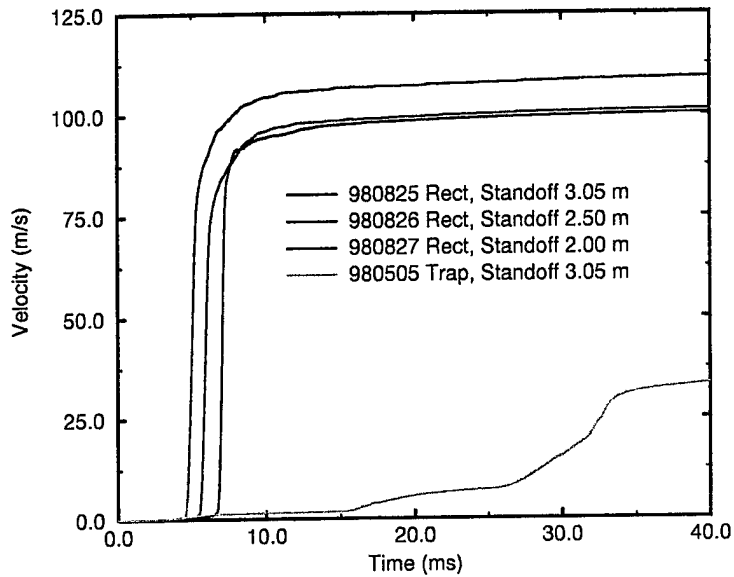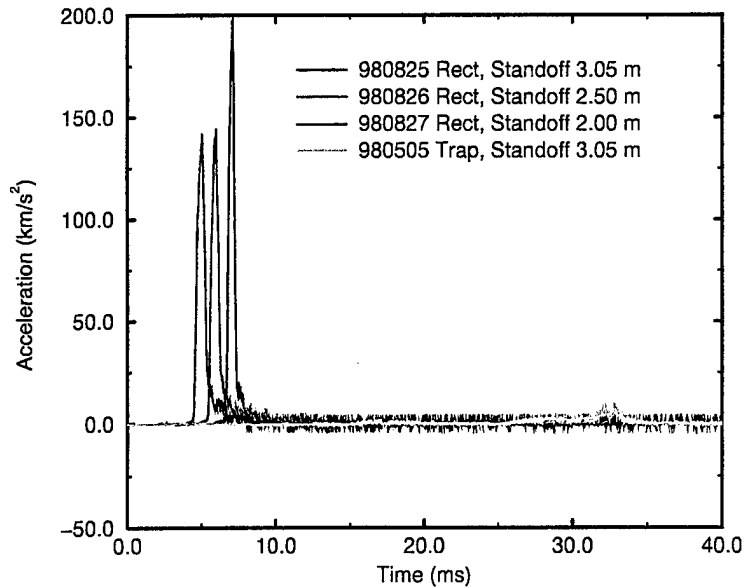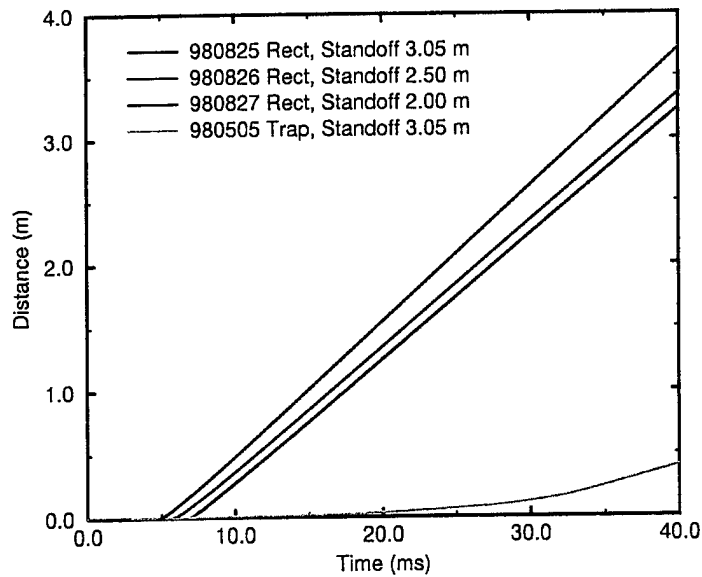

Figure 46. Acceptor Stack X-Direction Distance Moved, Computations 980825 Through 980827 (Rectangular), Plus 980505 (Trapezoidal).

53

for the acceptor stack in the preceding figures. The ordinate parameters are normalized in the same way as was done in Figure 39: the direct ratio of the respective parameters relative to the values for the 3.05-m standoff. The solid black momentum curve appears to be plotted as a dashed line because it is overlaid by the dashed red velocity curve. This is because of the simple scaling of the two curves by mass. Figure 48 shows the same ordinate data plotted against the inverse normalized standoff, with that normalization done in the same way as for Figures 40 and 41. Figure 49 is a rescaled version of Figure 48, with the scaling selected to exactly match that used for Figure 41 to facilitate comparison. Like the barricade, the acceptor stack parameters for peak momentum, velocity, total impulse, and distance at 40 ms are relatively weak direct functions of inverse standoff ratio, but the normalized peak acceleration shows a strong negative correlation with normalized inverse standoff.
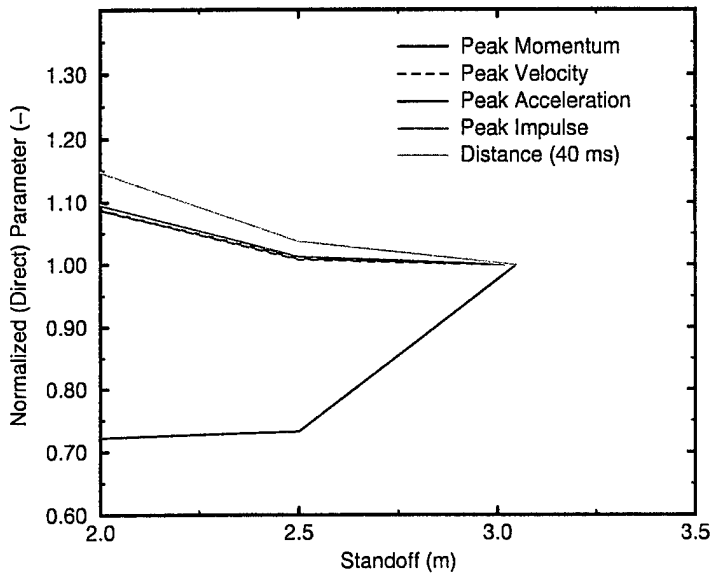
Figure 47. Normalized (Direct Ratio) Acceptor Stack Parameters Versus Standoff Distance, Computations 980825 Through 980827.

The simple standoff distance, measured from the stack base to the barricade base, may not be the only meaningful distance to consider when examining these parameters for the acceptor stack. The total distance between the right face of the donor stack and the left face of the acceptor stack, equal to twice the standoff plus the base width of the barricade, may be an informative parameter to use. For convenience, this distance is hereinafter referred to as "face separation." Figure 50 shows the ordinate values from Figures 47, 48, and 49 plotted against an abscissa showing the face separation. Figure 51 shows the same ordinate data plotted against the inverse normalized face separation. The normalizing value in the numer-

Figure 48. Normalized (Direct Ratio) Acceptor Stack Parameters Versus Normalized (Inverse Ratio) Standoff Distance, Computations 980825 Through 980827.
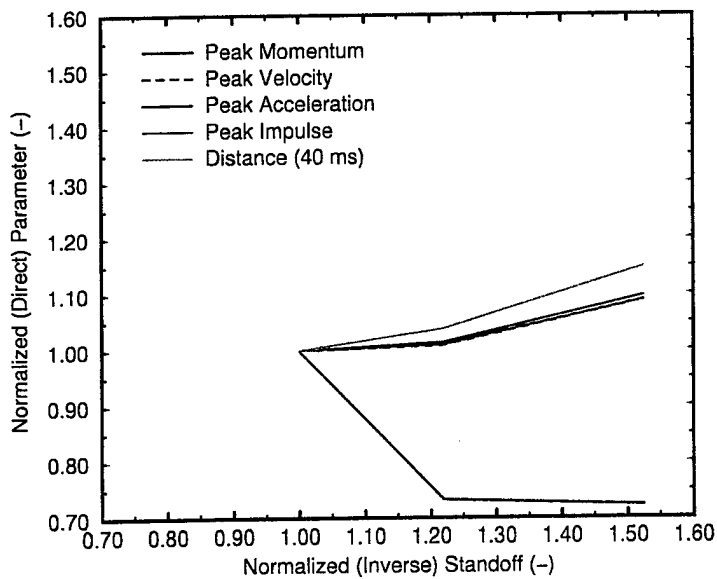
Figure 49. Normalized (Direct Ratio) Acceptor Stack Parameters Versus Normalized (Inverse Ratio) Standoff Distance (Rescaled), Computations 980825 Through 980827.

ator was the face separation for the 3.05 m standoff. One-to-one scaling for the normalized abscissa and ordinate was forced in this figure. The normalized peak momentum, velocity, impulse, and distance show a weak correlation with the inverse normalized face separation. The peak acceleration shows a relatively strong negative correlation with inverse normalized face separation.
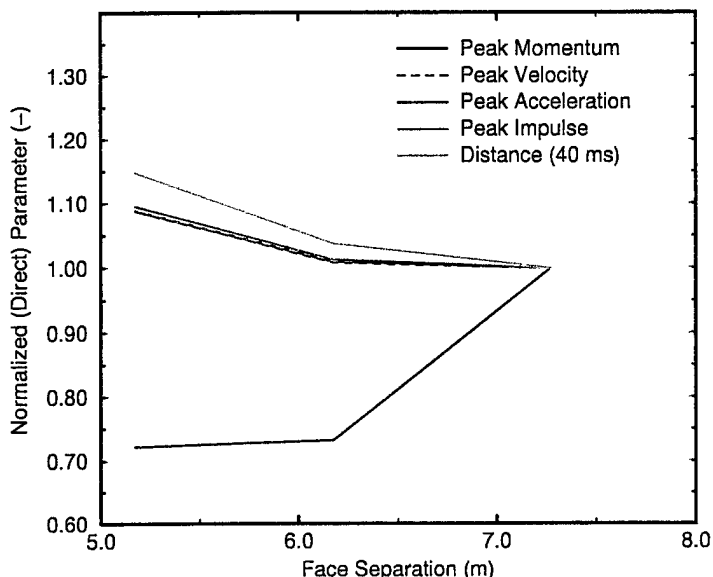
Figure 50. Normalized (Direct Ratio) Acceptor Stack Parameters Versus Face Separation. Computations 980825 Through 980827.

3.4. Acceptor Stack Left Surface Pressures

The pressures on the surface of the acceptor stack during this type of event are of great interest. Data from the 30 tracers that were placed uniformly along the left surface of the acceptor stack were processed to present a comprehensive summary of the overpressure history on that surface for each computation. An area-weighted average overpressure was computed using all of the 30 individual tracer pressures at each point in time. The maximum overpressure for any of the tracers at a given time was identified, as was the minimum. The results from the three computations for the thin rectangular barricade are presented here along with results from previous computations[2] for the massive trapezoidal water barricade at matching standoff distances: 980505 (3.05-m standoff), 980521 (2.50-m standoff), and 980610 (2.00-m standoff). Figure 52 shows the average, maximum, and minimum overpressures versus time on the left surface of the acceptor stack for a standoff of 3.05 m for Computation 980825, which has the thin rectangular barricade, and the average and maximum overpressures for
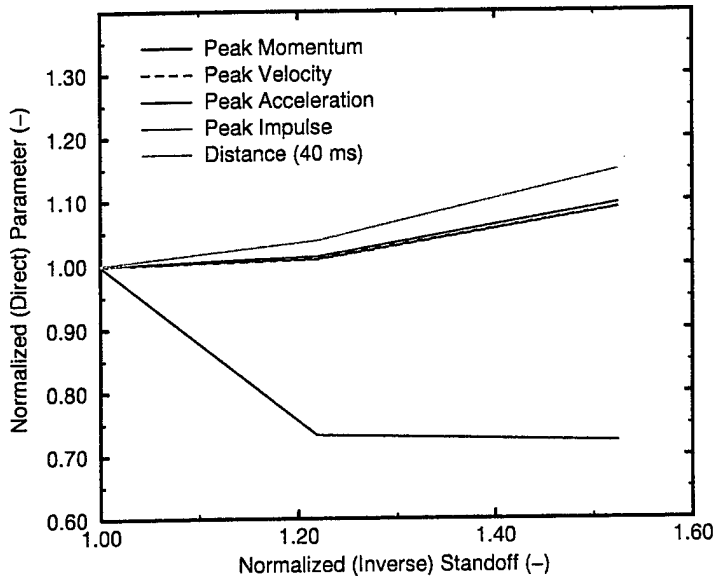
56
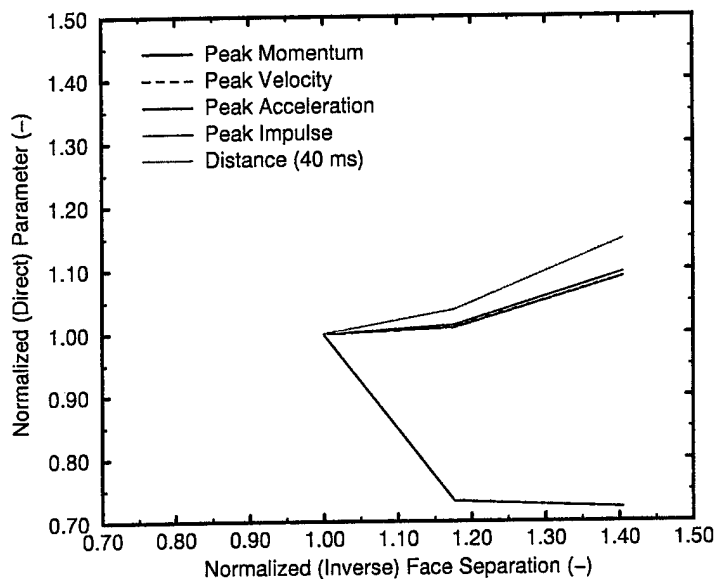
Figure 51. Normalized (Direct Ratio) Acceptor Stack Parameters Versus Normalized (Inverse Ratio) Face Separation, Computations 980825 Through 980827.

Computation 980505. The overpressure history for Computation 980825 is dominated by a single, large spike centered around 7 ms, with comparatively minor pressure activity after that. The early air shock at about 3 ms is negligible by comparison. The average and maximum overpressures for 980505 do not show as being significant on this plotting scale until about 15 ms, and are quite small compared with those for 980825. The average overpressure plot for 980825 in Figure 52 is particularly useful in helping to better understand the sharp rise of the impulse curve at early time to a near-maximum value for the 3.05-m standoff shown in Figure 45.

Figure 53 shows the plots of average, maximum, and minimum overpressure for 980826 along with corresponding plots of average and maximum overpressure for the trapezoidal barricade Computation 980521 at a 2.50-m standoff. Similarly, Figure 54 shows the same sets of plots for Computations 980827 (rectangular barricade) and 980610 (trapezoidal barricade). The overpressure values in these two plots show qualitatively similar behavior to that shown in Figure 52. All show an essentially negligible loading from the air shock at early time. Subsequently, the overpressure histories for the left face of the acceptor stack in the computations for the thin rectangular barricade are dominated by a single, large main pulse because of a broad-area impact of the barricade. Those for the trapezoidal barricade have a comparatively small two-stage overpressure loading because of a two-stage impact of the barricade on the acceptor stack, first on the top of the left face, and then an impact spreading upward from the bottom of the left face. All three computations for the thin rectangular

57

Figure 52. Acceptor Stack Left Surface Overpressure, 3.05-m Standoff, Computations 980825 (Rectangular) and 980505 (Trapezoidal).

water barricade show peak values of overpressure on the left surface of the acceptor stack in the range of 2 GPa (20 kbar). These are high enough pressures to represent a threat of inducing a chemical reaction in the acceptor stack if they are efficiently transmitted through packaging and/or casings to the energetic loads of the munitions. The report by Liddiard and Forbes[18] stated, for example, that the underwater sensitivity test (UST) showed that "...compression by a 3 or 4 kbar shock is, of itself, a sufficient external stimulus to start chemical reaction in a heterogeneous solid explosive such as pentolite..." and "...UST burning occurs at peak stresses of 4 to 12 kbar in the explosives..." These blast pressures on the simulated, flat iron surface of the acceptor stack are probably higher than they would be on a more realistically simulated surface of individual munitions with curved surfaces or individual boxes. Those lower surface pressures would transmit a further-reduced shock through the packaging and casing materials into the energetic load of the munitions in a real acceptor stack because of the probable impedance mismatches at the various interfaces. However, secondary impacts of accelerated munitions into other munitions could serve to generate increased pressures being generated at the impact interfaces. The addition of any impacts by fragments from the donor stack, not considered here, would introduce a new set of dynamics into the loading of the munitions in the acceptor stack.
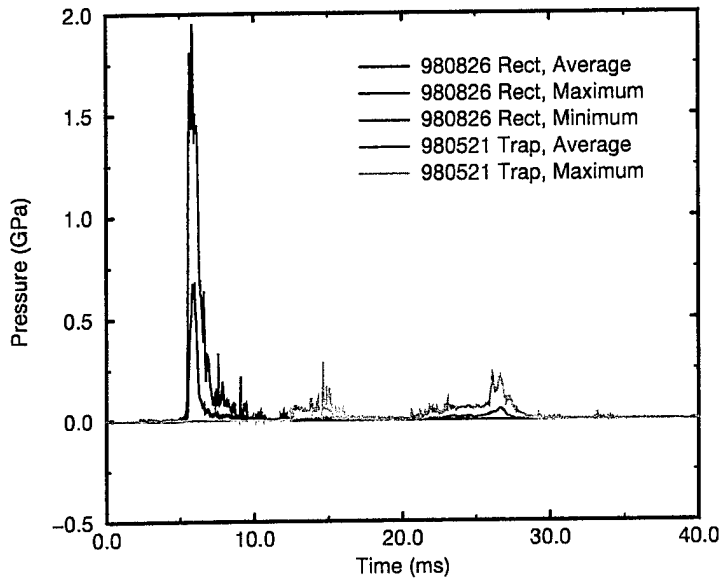
Figure 53. Acceptor Stack Left Surface Overpressure, 2.50-m Standoff, Computations 980826 (Rectangular) and 980521 (Trapezoidal).

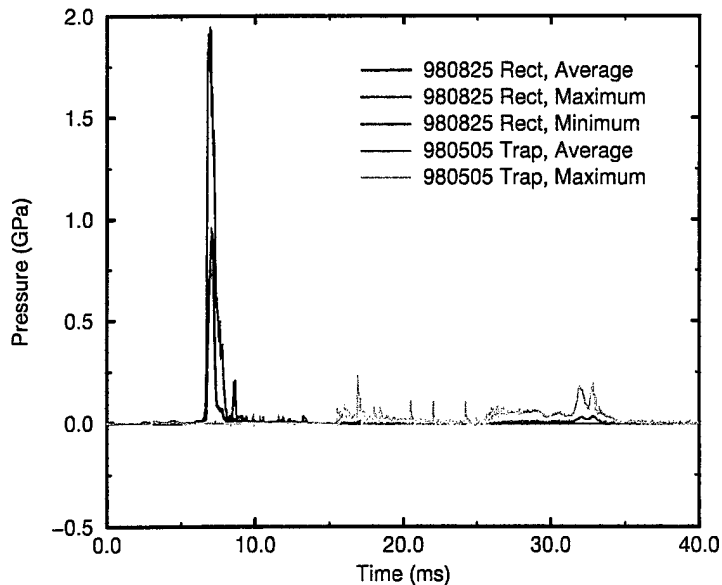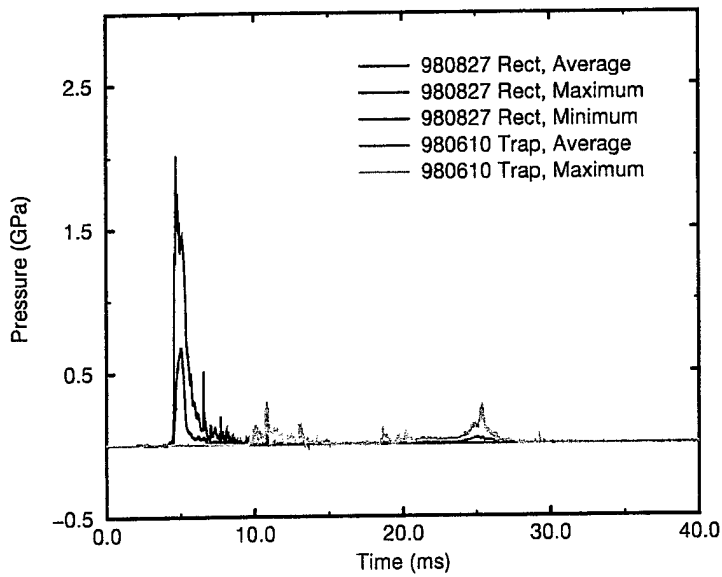

Figure 54. Acceptor Stack Left Surface Overpressure, 2.00-m Standoff, Computations 980827 (Rectangular) and 980610 (Trapezoidal).

4. CONCLUSION

The coupled computations discussed herein modeled a simplified, uncased, rectangular explosive charge representing a nominal munitions stack containing 4,000 kg of Comp-B undergoing a complete, high-order detonation with the initiation point at its center. No munitions casings or packing materials (and their resulting fragments) were included. The only barricade design that was used was a solid, water-only 1.17-m-thick rectangle. A geometrically simplified 2-D Cartesian coordinates system with the same finite-difference grid was used throughout the computations. This eliminated 3-D divergence effects that could reduce loadings considerably. The only parameter that was varied was the standoff distance.

These computations demonstrate a relatively weak inverse functional relationship between normalized values of the standoff distance and the loading on and whole-body response of the barricade. Similar results for both standoff and face separation were found for the loading on and whole-body response of the acceptor stack, except for a stronger functional relation of acceleration. The impact loading on the acceptor stack by the thin rectangular water barricade is much more severe than that reported earlier[2] for the massive trapezoidal water barricade. Peak pressures on the acceptor stack are high enough, approximately 2 GPa, to represent a threat of initiating a chemical reaction in munitions within the acceptor stack. Also, the rectangular barricade was not effective in keeping explosive products from the donor stack away from the acceptor stack. Because the donor stack was represented by a simple, bare explosive charge, the synergistic effects of the impact of large numbers of high-speed fragments along with the barricade impact loading were not addressed. Another series of computations for a 1.70-m-thick rectangular water barricade has been completed and will be reported promptly in a separate publication, and the results of all of the water barricade computations reported to date will be tied together. Additional computational studies of sand-filled barricades are in progress, as are studies of the impact of water and sand on simulated munitions.

60

REFERENCES

1. R.E. Lottero, "Responses of a Water Barricade and an Acceptor Stack to the Detonation of a Donor Munitions Stack," ARL-TR-1600, U.S. Army Research Laboratory, Aberdeen Proving Ground, MD, March 1998.

2. R.E. Lottero, "Standoff Variation Study I: Detonation of a Donor Munitions Stack and Responses of a Trapezoidal Water Barricade and an Acceptor Stack," ARL-TR-1943, U.S. Army Research Laboratory, Aberdeen Proving Ground, MD, May 1999.

3. J.M. McGlaun, S.L. Thompson, L.N. Kmetck, and M.G. Elrick, "A Brief Description of the Three-Dimensional Shock Wave Physics Code CTH," SAND 89-0607, Sandia National Laboratories, Albuquerque, NM, July 1990.

4. R.L. Bell, M.R. Baer, R.M. Brannon, M.G. Elrick, E.S. Hertel Jr., S.A. Silling, and P.A. Taylor, "CTHGEN User's Manual and Input Instructions, Version 4.00," CTH Development Project, Sandia National Laboratories, Albuquerque, NM, 10 March 1998.

5. R.L. Bell, M.R. Baer, R.M. Brannon, M.G. Elrick, E.S. Hertel Jr., S.A. Silling, and P.A. Taylor, "CTH User's Manual and Input Instructions, Version 4.00," CTH Development Project, Sandia National Laboratories, Albuquerque, NM, 13 March 1998.

6. J. Starkenberg, K.J. Benjamin, and R.B. Frey, "Predicting Fragmentation Propagation Probabilities for Ammunition Stacks," ARL-TR-949, U.S. Army Research Laboratory, Aberdeen Proving Ground, MD, January 1996.

7. Headquarters, Department of the Army, "Technical Manual. Army Ammunition Data Sheets. Artillery Ammunition. Guns, Howitzers, Mortars, Recoilless Rifles, Grenade Launchers, and Artillery Fuzes." TM-43-0001-28, April 1977.

8. Department of the Army, "Ammunition and Explosives Safety Standards," AR 385-64, 22 May 1987.

9. G.I. Kerley and T.L.C. Frear, "Composition B-3 Detonation Products," SAND93-2131, Sandia National Laboratories, Albuquerque, NM, 1993.

10. G.I. Kerley, "CTH Reference Manual: The Equation of State Package," SAND91-0344, Sandia National Laboratories, Albuquerque, NM, 24 May 1991.

11. B.M. Dobratz and P.C. Crawford, "LLNL Explosives Handbook, Properties of Chemical Explosives and Explosive Simulants," UCRL-52997, Change 2, Lawrence Livermore National Laboratory, Livermore, CA, 31 January 1985.

12. Hesco Bastion Limited, Unit 37, Knowsthorpe Gate, Cross Green Industrial Estate, Leeds LS9 ONP, West Yorkshire, England.

13. J. Starkenberg, Private communication, U.S. Army Research Laboratory, Aberdeen Proving Ground, MD, July 1998.

61

14. R.D. Cregar, Private communication, U.S. Army Research Laboratory, Aberdeen Proving Ground, MD, July 1998.

15. F.H. Ree, "Equation of State for Water," UCRL-52190, Lawrence Livermore National Laboratory, Livermore, CA, December 1976.

16. G.I. Kerley, "Multiphase Equation of State for Iron," SAND93-0227, Sandia National Laboratories, Albuquerque, NM, 1993.

17. H.C. Graboske, Data for dry air, UCID-16901, December 1981 (modified March 1992).

18. T.P. Liddiard and J.W. Forbes, "A Summary Report of the Modified Gap Test and the Underwater Sensitivity Test," NSWC TR 86-350, Naval Surface Warfare Center, Silver Spring, MD, 12 March 1987.

NO. OF COPIES	ORGANIZATION	NO. OF COPIES	ORGANIZATION
2	DEFENSE TECHNICAL INFORMATION CENTER DTIC DDA 8725 JOHN J KINGMAN RD STE 0944 FT BELVOIR VA 22060-6218	1	DIRECTOR US ARMY RESEARCH LAB AMSRL DD J J ROCCHIO 2800 POWDER MILL RD ADELPHI MD 20783-1145
1	HQDA DAMO FDQ D SCHMIDT 400 ARMY PENTAGON WASHINGTON DC 20310-0460	1	DIRECTOR US ARMY RESEARCH LAB AMSRL CS AS (RECORDS MGMT) 2800 POWDER MILL RD ADELPHI MD 20783-1145
1	OSD OUSD(A&T)/ODDDR&E(R) R J TREW THE PENTAGON WASHINGTON DC 20301-7100	3	DIRECTOR US ARMY RESEARCH LAB AMSRL CI LL 2800 POWDER MILL RD ADELPHI MD 20783-1145

NO. OF COPIES	ORGANIZATION
1	DPTY CG FOR RDE HQ US ARMY MATERIEL CMD AMCRD MG CALDWELL 5001 EISENHOWER AVE ALEXANDRIA VA 22333-0001
1	INST FOR ADVNCD TCHNLGY THE UNIV OF TEXAS AT AUSTIN PO BOX 202797 AUSTIN TX 78720-2797
1	DARPA B KASPAR 3701 N FAIRFAX DR ARLINGTON VA 22203-1714
1	NAVAL SURFACE WARFARE CTR CODE B07 J PENNELLA 17320 DAHLGREN RD BLDG 1470 RM 1101 DAHLGREN VA 22448-5100
1	US MILITARY ACADEMY MATH SCI CTR OF EXCELLENCE DEPT OF MATHEMATICAL SCI MAJ M D PHILLIPS THAYER HALL WEST POINT NY 10996-1786

ABERDEEN PROVING GROUND

4	DIR USARL AMSRL CI LP (305)

NO. OF COPIES	ORGANIZATION	NO. OF COPIES	ORGANIZATION
1	DIRECTOR DEFENSE RSCH AND ENGNRNG DD TWP WASHINGTON DC 20301	1	OFFICER IN CHARGE CIVIL ENGNRNG LAB NAVAL CONST BATTALION CTR TECH LIB CODE L31 PORT HUENEME CA 93041
1	COMMANDER FIELD COMMAND DSWA FCTTS E MARTINEZ KIRTLAND AFB NM 87115	1	COMMANDER NAVAL WEAPONS CTR TECH LIB CODE 533 CHINA LAKE CA 93555-6001
1	DIRECTOR ADV RSCH PROJECTS AGNCY TECH LIB 3701 N FAIRFAX DR ARLINGTON VA 22203-1714	1	COMMANDER NSWC DAHLGREN DIVISION LIB CODE E23 DAHLGREN VA 22448-5000
1	COMMANDER USA ARDEC AMSTA FSM W BARBER BLDG 94 PICATINNY ARSENAL NJ 07806-5000	1	COMMANDER NAVAL RSCH LAB TECH LIB CODE 2027 WASHINGTON DC 20375
1	COMMANDER USA ENGINEER DIVISION HNDED FD PO BOX 1500 HUNTSVILLE AL 35807	1	COMMANDER NAVAL WEAPOONS EVAL FAC DOCUMENT CONTROL KIRTLAND AFB NM 87117
1	COMMANDER USA CORPS OF ENGNRS FT WORTH DSTRCT CESWF PM J PO BOX 17300 FT WORTH TX 76102-0300	2	AIR FORCE ARMAMENT LAB AFATL DOIL AFATL DLYV EGLIN AFB FL 32542-5000
1	COMMANDER USA RSCH OFFICE SLCRO D PO BOX 12211 RESEARCH TRIANGLE PARK NC 27709-2211	1	DIRECTOR LAWRENENC LIVERMORE NATL LAB TECH INFO DEPT L 3 PO BOX 808 LIVERMORE CA 94550
1	COMMANDER DAVID TAYLOR RSCH CTR TECH INFO CTR CODE 522 BETHESDA MD 20084-5000	1	NAIC DXLA TECH LIB 4180 WATSON WAY WRIGHT PATTERSON AFB OH 45433-5648
		1	KAMAN SCIENCES CORPORATION LIBRARY PO BOX 7463 COLORADO SPRINGS CO 80933-7463

NO. OF COPIES	ORGANIZATION	NO. OF COPIES	ORGANIZATION
1	DIRECTOR SANDIA NATL LAB DOC CONTROL 3141 PO BOX 5800 ALBUQUERQUE NM 87185-5800	3	SOUTHWEST RSCH INSTITUTE C ANDERSON S MULLIN A B WENZEL PO DRAWER 28255 SAN ANTONIO TX 78228-0255
2	LOS ALAMOS NATL LAB RPT COLCTN CIC 14 MS P364 CID 14 MS P364 PO BOX 1663 LOS ALAMOS NM 87545	1	UNIVERSITY OF TEXAS ARL ELCTROMAG GROUP A TUCKER CAMPUS MAIL CODE F0250 AUSTIN TX 78712
1	REPORT COLLECTION AGENCY RSCH LAB MS P362 PO BOX 7113 LOS ALAMOS NM 87544-7113	1	UNIV OF MARYLAND R DICK RM 2168 ENGRG CLASSROOM BLDG COLLEGE PARK MD 20742-5121
1	DIRECTOR SANDIA NATL LAB LIVERMORE LAB DOC CONTROL FOR THE LIB PO BOX 969 LIVERMORE CA 94550	1	US NAVAL ACADEMY TECH LIB 572 HOLLOWAY RD ANNAPOLIS MD 21402-5002
1	DIRECTOR NASA LANGLEY RSCH CTR TECH LIB HAMPTON VA 23665	1	OLIN ORDNANCE RECH LIB J KIBIGER PRODUCT MATERIAL CONTROL 10101 9TH ST N ST PETERSBURG FL 33716
1	SUNBURST RECOVERY INC C YOUNG PO BOX 2129 STEAMBOAT SPRINGS CO 80477	1	COMMANDER INDIAN HEAD DIV NSWC CODE 950T M SWISDAK 101 STRAUSS AVE INDIAN HEAD MD 20640-5035
2	SRI INTERNATIONAL J GRAN B HOLMES 333 RAVEWOOD AVE MENLO PARK CA 94025	1	COMMANDING OFFICER NFESC J TANCRETO ESC62 1100 23RD AVE BLDG 1100 PORT HUENEME CA 93043-4370
2	DENVER RSCH INSTITUTE J WISOTSKI TECH LIB PO BOX 10758 DENVER CO 80210	1	CHAIRMAN DOD EXPOSIVES SAFETY BOARD J WARD HOFFMAN BLDG 1 ROOM 856C 2461 EISENHOWER AVE ALEXANDRIA VA 22331-0600

NO. OF COPIES	ORGANIZATION	NO. OF COPIES	ORGANIZATION
1	DEFENSE AMMOLOG ACTIVITY AMSTA AR AL D SCARBOROUGH PICATINNY ARSENAL NJ 07806-5000		ABERDEEN PROVING GROUND
		1	COMMANDER US ARMY TECOM AMSTE TE F L TELETSKI
1	US ARMY SOLDIER SYSTEMS CMD SSCNS WSO D LEMOINE KANSAS ST NATICK MA 01760-5018	1	COMMANDER USATC STEC LI

5	USAE WATERWAYS EXP STN
	CEWES SD R
	P KINNEBREW
	B CARNES
	CEWES TL TECH LIB
	CEWES SD K DAVIS
	CEWES SS J WEATHERSBY
	3909 HALLS FERRY RD
	VICKSBURG MS 39180-6199
		29	DIR USARL
			AMSRL WM MA
			  W CHIN
			  T MULKERN
			  C PERGANTIS
			AMSRL WM PB
			  B GUIDOS
			  H EDGE
			  P PLOSTINS
			  P WEINACHT
			AMSRL WM T
			  A M DIETRICH
			AMSRL WM TB
			  V BOYLE
			  P BAKER
			  T DORSEY
			  R FREY
			  W HILLSTROM
			  W LAWRENCE
			  R LOTTERO (5CPS)
			  E MCDOUGAL
			  J STARKENBERG
			  J WATSON
			AMSRL WM TC
			  K KIMSEY
			  D SCHEFFLER
			  S SCHRAML
			AMSRL WM TD
			  P KINGMAN
			  M RAFTENBERG
			  S SCHOENFELD
			  P SIMMERS

1	DIR SNL ES HERTEL JR MS 0819 PO BOX 5800 ALBUQUERQUE NM 87185-0307		
1	KERLEY PUB SUC G I KERLEY PO BOX 13835 ALBUQUERQUE NM 87192-3835		

1. AGENCY USE ONLY *(Leave blank)*	2. REPORT DATE May 1999	3. REPORT TYPE AND DATES COVERED Final, 1 Jan 98 - 31 Jan 99	
4. TITLE AND SUBTITLE Standoff Variation Study I: Detonation of a Donor Munitions Stack and Responses of a Thin Rectangular Water Barricade and an Acceptor Stack			**5. FUNDING NUMBERS** JONO: 9810F1
6. AUTHOR(S) Richard E. Lottero			
7. PERFORMING ORGANIZATION NAME(S) AND ADDRESS(ES) U.S. Army Research Laboratory ATTN: AMSRL-WM-TB Aberdeen Proving Ground, MD 21005-5066			**8. PERFORMING ORGANIZATION REPORT NUMBER** ARL-TR-1948
9. SPONSORING/MONITORING AGENCY NAMES(S) AND ADDRESS(ES)			**10. SPONSORING/MONITORING AGENCY REPORT NUMBER**
11. SUPPLEMENTARY NOTES			
12a. DISTRIBUTION/AVAILABILITY STATEMENT Approved for public release; distribution is unlimited.			**12b. DISTRIBUTION CODE**

13. ABSTRACT *(Maximum 200 words)*

This report documents the second stage of the continuation of the fully coupled numerical modeling of the detonation of a simplified munitions stack in a temporary storage area and the subsequent effects on the immediate surroundings of the stack. Three plausible configurations of this munitions stack, referred to as the "donor" stack, an intervening water barricade, and an "acceptor" munitions stack are modeled in two-dimensional (2-D) Cartesian hydrocode computations using the CTH hydrodynamics computer code. The distance between each munitions stack and the barricade, referred to here as the "standoff" distance, is varied from one computation to the next, with the physical characteristics of the munitions stacks and barricade themselves remaining unchanged. The donor stack is modeled as an uncased condensed high-explosive charge with a rectangular cross section. The water barricade has a relatively thin rectangular cross section, and the acceptor stack is a solid iron rectangle. The loadings on both the barricade and the acceptor stack are computed, as are their fully coupled responses to those loadings. Only a relatively weak inverse functional relationship with standoff distance was found in the barricade response. Weak correlations with both standoff distance and face separation were also found for all parameters that were evaluated for the acceptor stack response, except for the whole-body acceleration. The results are also compared with those of the first part of this study on the coupled blast loading and response computations for a massive water barricade with a trapezoidal cross section.

14. SUBJECT TERMS munitions survivability, detonation modeling, barricade, blast loading, hydrocode			15. NUMBER OF PAGES 76
			16. PRICE CODE
17. SECURITY CLASSIFICATION OF REPORT UNCLASSIFIED	**18. SECURITY CLASSIFICATION OF THIS PAGE** UNCLASSIFIED	**19. SECURITY CLASSIFICATION OF ABSTRACT** UNCLASSIFIED	**20. LIMITATION OF ABSTRACT** UL

INTENTIONALLY LEFT BLANK.

USER EVALUATION SHEET/CHANGE OF ADDRESS

This Laboratory undertakes a continuing effort to improve the quality of the reports it publishes. Your comments/answers to the items/questions below will aid us in our efforts.

1. ARL Report Number/Author_____ARL-TR-1948 (Lottero)_____ Date of Report __May 1999_____

2. Date Report Received _____

3. Does this report satisfy a need? (Comment on purpose, related project, or other area of interest for which the report will be used.) _____

_____

_____

4. Specifically, how is the report being used? (Information source, design data, procedure, source of ideas, etc.) _____

_____

_____

5. Has the information in this report led to any quantitative savings as far as man-hours or dollars saved, operating costs avoided, or efficiencies achieved, etc? If so, please elaborate. _____

_____

_____

6. General Comments. What do you think should be changed to improve future reports? (Indicate changes to organization, technical content, format, etc.) _____

_____

_____

_____

_____

Organization

CURRENT   Name   E-mail Name
ADDRESS
              _____
              Street or P.O. Box No.

              _____
              City, State, Zip Code

7. If indicating a Change of Address or Address Correction, please provide the Current or Correct address above and the Old or Incorrect address below.

              _____
              Organization

OLD   Name
ADDRESS
              _____
              Street or P.O. Box No.

              _____
              City, State, Zip Code

(Remove this sheet, fold as indicated, tape closed, and mail.)
(DO NOT STAPLE)